[33]L. M. Branscomb and S. J. Smith, Phys. Rev. 98, 1028 (1955).
[34]K. T. Chung and R. P. Hurst, Phys. Rev. 152, 35 (1966).
[35]C. L. Pekeris, Phys. Rev. 126, 1470 (1962).

PHYSICAL REVIEW A VOLUME 4, NUMBER 2 AUGUST 1971

Spectroscopy and Collision Theory. The Xe Absorption Spectrum*†

K. T. Lu‡
Department of Physics, The University of Chicago, Chicago, Illinois 60637
(Received 5 February 1971)

Experiments on the uv photoabsorption of Xe have determined level positions, line intensities, Landé g factors, intensity profiles in the auto-ionization region, and the branching ratio of photoelectron groups. This paper expresses all these data in terms of a single set of theoretical parameters which pertain to collisions of the $e+Xe^+$ system with $J=1$ and characterize the five close-coupling eigenchannels of this system. Values of the parameters, obtained by fitting the experimental data, provide (1) values of the zero-energy scattering eigenphases, (2) evidence that the orbital angular momentum of the free electron ($l=0$ or 2) is a good quantum number to within ~2%, and (3) evidence that the LS coupling classification of the $e+Xe^+$ complex holds approximately, but only for $l=2$. The whole analysis correlated diverse experimental data into a unified pattern and can be extended to other values of J and l to other rare gases and to spectra of other elements.

I. INTRODUCTION

Theorems describing connections between photoabsorption in discrete and continuum spectra have been established for some time.[1] More generally, the wave functions of continuum states of an electron-ion system, which represent electron-ion collisions, are closely related to those of the discrete states studied by ordinary spectroscopy. This relationship is rather simple when the ion has a closed-shell structure as in an alkaline atom. The electron's motion outside the ion is then represented by a Coulomb wave function with a quantum defect μ, equivalent to a phase shift $\delta=\pi\mu$, and the relationship between the discrete and continuum wave function is rather well known. (The effects of core polarization can also be taken into account but will be disregarded in this paper.) The situation is more complicated for open-shell ions with two or more low-lying levels, but the necessary theory has been developed, notably in the form of a multichannel QDT (quantum-defect theory).[2] However, little information on collision processes has been extracted thus far from the wealth of spectroscopic data, nor have these data been fitted extensively into the broader point of view of collision theory.

Fano in a recent paper,[3] referred to in the following as FH, has interpreted a highly perturbed portion of the H_2 spectrum by collision theory. The electron-ion system was treated in that paper with emphasis on eigenstates of the combined system rather than in terms of a nondiagonal reaction matrix[2,4] which describes the interaction between closed and open channels. The application of the method of FH to the analysis of perturbed atomic spectra has been outlined in a preliminary paper[5] which will be called LF. Here we apply the method of FH to a detailed analysis of the photoabsorption of Xe.

Photoabsorption by Xe in its ground state leads to $(5p^5)d$ or $(5p^5)s$, $J=1$, odd-parity states belonging to five series (or channels), of which three converge to the first ionization limit $I_{3/2}$ and two converge to the second ionization limit $I_{1/2}$. The thresholds $I_{3/2}$ and $I_{1/2}$ correspond to the $(5p^5)\,^2P_{3/2,1/2}$ ground-state doublet of the ion. In the discrete spectrum some of these series are so strongly perturbed as to be hardly identifiable. In the auto-ionization region between the two limits, levels converging to $I_{1/2}$ have auto-ionization widths comparable to the level separations. Photons with energy $h\nu$ above the second threshold produce photoelectrons with two energies $h\nu-I_{3/2}$ and $h\nu-I_{1/2}$; the measured value[6] of the branching ratio of the two energy groups is ~1.6:1 instead of the "statistical" ratio of 2:1.

We propose here to analyze all the available data on $J=1$ level positions,[7] on the intensities of absorption lines,[8] on the intensity profiles in the Beutler spectrum,[9] on the photoelectron group ratio,[6] and on the Landé g factors[10] from the point of view of collision theory. In this work, level positions and spectral intensities will be expressed analytically and plotted as functions of an effective quantum number $\nu_{1/2}$. The analytical expressions will consist mainly of trigonometric functions of $\pi\nu_{1/2}$, invariant under the transformation $\nu_{1/2}\to\nu_{1/2}+n$. This invariance accounts for the periodicity of

Rydberg series. Conversely, it permits us to pool the experimental evidence provided by levels with quite different values of $\nu_{1/2}$ on plots covering just one unit's range of this parameter.

These data, which pertain to photoabsorption occurring below, between, and above the ionization limits, will be expressed in terms of a single set of theoretical parameters. The parameters are determined here by fitting to experimental data, but they have a well-defined meaning and should be the objective of future theoretical calculations. Note that these parameters are dimensionless, as are the phase shifts and the interaction and reaction matrix elements of collision theory. The interaction parameters of theoretical spectroscopy often have the dimension of energy but generally they can be made dimensionless and comparable to the parameters of collision theory by a change of normalization.[11]

The calculations reported in this paper are frankly exploratory. They aim at demonstrating qualitative relationships and at evaluating parameters to one- or two-digit accuracy only. One main limitation on accuracy should be explained at the outset: All parameters of QDT's depend on the total energy of the system, but their variations over an energy interval ΔE are of order $\Delta E/I_{3/2}$. These variations are disregarded in the present work, as they were in FH, even though a part of them is predicted by the QDT (see, e.g., Appendix B of FH) and the rest could be allowed for by fitting of linear regressions. The energy range ΔE over which the theory is of interest is a few times the separation of thresholds $I_{1/2}-I_{3/2}$ which is, in turn, $\sim 0.1 I_{3/2}$ for Xe. Hence $\Delta E/I_{3/2}$ is not really negligible in this paper, while it was small in FH. Nevertheless only limited evidence has emerged of gross errors due to disregarding $\Delta E/I_{3/2}$.

II. QUANTUM-DEFECT THEORY

Consider initially an excited or ionized stationary state of an alkaline (or other) atom with a closed-shell ionic core. We express the energy of this state, in atomic units, by

$$E = I - 1/2\nu^2 = I + \tfrac{1}{2}k^2 , \tag{2.1}$$

where I represents the energy of the ionic core. For distances of the excited electron sufficiently far away from the nucleus, $r > r_0$, such that the electron is outside the core and is only subject to Coulomb attraction, the wave function of the atom can be written as

$$\Psi = \Phi[f(\nu, r)c - g(\nu, r)d] . \tag{2.2}$$

Here Φ represents the state of the core, of all spins, and the rotational part of the excited electron's wave function; f and g are standard Coulomb wave functions described in Sec. III of FH and in Ref. 2; and c and d are coefficients described below. Symmetrization of the coordinate r of the excited electron with those of other electrons included in Φ is implied in (2.2), though not indicated explicitly.

The interaction of the electron with the ionic core, in the non-Coulomb zone $r < r_0$, is *fully represented* in this problem by a boundary condition at $r = r_0$ which sets the coefficients of (2.2) at

$$c = \cos\pi\mu , \quad d = \sin\pi\mu . \tag{2.3}$$

Here μ indicates a quantum defect which is regarded in this paper as independent of the energy E over a sufficient range.[12] Above the ionization threshold, i.e., for $E > I$ and $\nu = i/k$, the wave functions f and g become

$$(2/\pi k)^{1/2}\sin(kr+\theta) \quad \text{and} \quad -(2/\pi k)^{1/2}\cos(kr+\theta) ,$$

respectively, with

$$\theta = -\tfrac{1}{2}l\pi + (1/k)\ln(2kr) + \arg\Gamma(l+1-i/k) .$$

The wave function (2.2) is then a continuum wave function normalized per unit energy range, with phase shift $\delta = \pi\mu$. Accordingly, the scattering matrix of the electron-ion collision problem is represented by its single element $e^{2i\pi\mu}$.

The cross section for photo-ionization is proportional to the squared dipole moment

$$D = \int \Psi_f^{\dagger}(\textstyle\sum_i z_i)\Psi_0 \, d\tau , \tag{2.4}$$

where Ψ_0 is the ground-state wave function of the atom, Ψ_f is the final-state wave function that coincides with (2.2) for $r > r_0$, and $d\tau$ represents integration over all electron positions $\vec{r}_i$. The dipole moment D thus defined is treated here as practically independent of E. The spectral density of oscillator strength is

$$\frac{df}{dE} = 2(E - E_0)|D|^2 , \tag{2.5}$$

where E_0 is the ground-state energy (in atomic units).

The Rydberg states of the discrete spectrum are identified by the condition that (2.2) remains finite at $r = \infty$ for $E < I$. For $E < I$ and large r the functions f and g are conveniently represented as superpositions of a rising exponential function $u(\nu, r)$ and a falling exponential $v(\nu, r)$ defined by Eq. (11) of FH,

$$\left.\begin{aligned} f &\to u(\nu, r)\sin\pi\nu - v(\nu, r)e^{i\pi\nu} \\ g &\to -u(\nu, r)\cos\pi\nu + v(\nu, r)e^{i\pi(\nu+1/2)} \end{aligned}\right\} \text{ as } r \to \infty . \tag{2.6}$$

Substituting (2.3) and (2.6) in (2.2), we have

$$\Psi \xrightarrow[\text{large } r]{} \Phi\{u(\nu, r)\sin\pi(\nu+\mu) - v(\nu, r)e^{i\pi(\nu+\mu)}\} . \tag{2.7}$$

The condition that Ψ remains finite at $r \to \infty$ is then

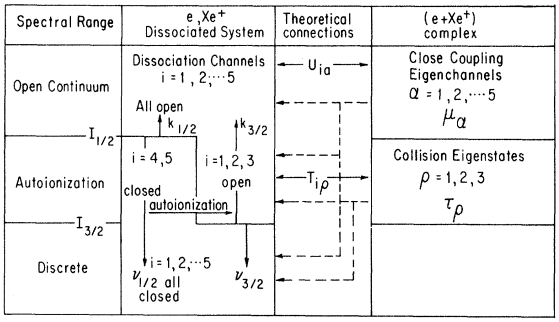

FIG. 1. Relationship between dissociation channels i and close-coupling eigenchannels α.

$$\sin\pi(\nu+\mu)=0\ ,\quad \text{i.e.,}\quad \nu=\nu_n=n-\mu\ . \tag{2.8}$$

Normalization of (2.2) in the discrete is obtained by multiplying (2.2) by $\nu_n^{-3/2}$ (see, e.g., Secs. VIB and VIC of FH). The oscillator strength of the nth line is then given by

$$f_n=2(E_n-E_0)|D|^2(1/\nu_n^3)\ . \tag{2.9}$$

Thus all characteristics of the absorption spectrum, over an energy range of the order of eV on either side of threshold, are represented by the two parameters μ and D in this simple case.

In the case of Xe there are two ionization limits $I_{3/2}$ and $I_{1/2}$, separated by ~1 eV, and thus two values $\nu_{3/2}$ and $\nu_{1/2}$, or $k_{3/2}$ and $k_{1/2}$, for each energy E. Equation (2.1) now takes the alternative forms

$$\begin{aligned}E&=I_{3/2}-1/2\nu_{3/2}{}^2=I_{3/2}+\tfrac{1}{2}k_{3/2}{}^2\\&=I_{1/2}-1/2\nu_{1/2}{}^2=I_{1/2}+\tfrac{1}{2}k_{1/2}{}^2\ .\end{aligned} \tag{2.10}$$

Note particularly that this equation establishes a functional relation between $\nu_{3/2}$ (or $k_{3/2}$) and $\nu_{1/2}$ (or $k_{1/2}$).

The absorption spectrum involves, as indicated in Sec. I, five wave functions Ψ_i of the form (2.2), with $i=1, 2, \ldots 5$. Here the analytic form of $f(\nu,r)$ and $g(\nu, r)$ in Eq. (2.2) remains independent of i, but ν, Φ, c, and d depend now on i. These five channels i, corresponding to a dissociated state of Xe^+ and e, will be identified by the jj coupling which is assumed for the functions Φ_i, as follows:

$$\begin{aligned}i=\quad &1 \qquad 2 \qquad 3\\ &[^2P_{3/2}]d_{5/2}\ ,\ [^2P_{3/2}]d_{3/2}\ ,\ [^2P_{3/2}]s_{1/2}\ ,\\ &\qquad\qquad 4 \qquad 5\\ &\qquad\qquad [^2P_{1/2}]d_{3/2}\ ,\ [^2P_{1/2}]s_{1/2}\end{aligned}\ , \tag{2.11}$$

where the $(5p)^5$ configuration of the Xe^+ ion and the total $J=1$ of each channel are implied. The value of $\nu_i=i/k_i$ coincides with $\nu_{3/2}$ for $i=1$, 2, and 3 and with $\nu_{1/2}$ for $i=4$, 5. In Xe problem, all five i channels are closed in the discrete spectrum, three channels $i=1$, 2, 3 are open and two channels $i=4$, 5 are closed in the auto-ionization region, and all five channels are open in the open continuum. These relationships are indicated on the left-hand side of Fig. 1. The determination of the coefficients c_i and d_i, on the basis of the electron-ion interaction for $r<r_0$, constitutes a main part of our problem. The interaction prevents a separate determination of c_i and d_i for each channel i. Rather we must consider a wave function

$$\Psi=\textstyle\sum_i\Phi_i[f(\nu_i, r)c_i-g(\nu_i, r)d_i]\ , \tag{2.12}$$

and c_i and d_i will be determined by the interplay of boundary conditions at $r=r_0$ and at $r\to\infty$.

Collision theory represents the effects of the short-range electron-ion interaction by a scattering matrix S_{ij}. At energies $E>I_{1/2}$, an electron incident on the ion in the jth channel with kinetic energy $\frac{1}{2}k_j^2$, with $J=1$ and odd parity, has probability amplitude S_{ij} of emerging from the collision in the ith channel with kinetic energy $\frac{1}{2}k_i^2$ but with the same *total* energy E. The 5×5 matrix S_{ij} with eigenvalues $e^{2i\pi\mu_\alpha}$ is diagonalized by a unitary transformation $U_{i\alpha}$,

$$e^{2i\pi\mu_\alpha}\delta_{\alpha\beta}=\sum_{ij}U^\dagger_{\alpha i}S_{ij}U_{j\beta} \tag{2.13}$$

or

$$S_{ij}=\sum_\alpha U_{i\alpha}e^{2i\pi\mu_\alpha}U^\dagger_{\alpha j}\ . \tag{2.14}$$

The five eigenphase shifts $\pi\mu_\alpha$ and the matrix $U_{i\alpha}$ characterize the close-coupling non-Coulomb interaction between electron and ion which prevails at short ranges. Each matrix element $U_{i\alpha}=(i|\,\alpha)$ connects the ith channel of the dissociated system consisting of e and Xe^+ to the αth "close-coupling eigenchannel" of the $e+Xe^+$ complex. The αth column of the matrix $U_{i\alpha}$ represents the αth eigenvector of the scattering matrix S_{ij}. In this paper $U_{i\alpha}$ is taken to be real, such that $U^\dagger_{\alpha i}=U_{i\alpha}$.

A close-coupling eigenfunction Ψ_α is a superposition of standing waves of all channels i with the *same eigenphase shift* $\pi\mu_\alpha$. This eigenfunction is obtained by setting

$$c_i=U_{i\alpha}\cos\pi\mu_\alpha\ ,\quad d_i=U_{i\alpha}\sin\pi\mu_\alpha \tag{2.15}$$

in the wave function (2.12), which becomes[13]

$$\begin{aligned}\Psi_\alpha=&[\textstyle\sum_i\Phi_i f(\nu_i, r)U_{i\alpha}]\cos\pi\mu_\alpha\\&-[\textstyle\sum_i\Phi_i g(\nu_i, r)U_{i\alpha}]\sin\pi\mu_\alpha\ .\end{aligned} \tag{2.16}$$

There is one such eigenfunction for each eigenvalue $e^{2i\pi\mu_\alpha}$ of the S matrix and for each total energy value E. Photo-ionization to each α state depends on the dipole matrix element D_α, i.e., on the value of (2.4) calculated for the state Ψ_f whose wave function coincides with Ψ_α for $r>r_0$.

The QDT is based on the fact that the short-range electron-ion interaction is represented by the same

parameters μ_α and $U_{i\alpha}$ throughout the spectral range of interest to us, i.e., for energies E from below the threshold $I_{3/2}$ to above the threshold $I_{1/2}$. These parameters are slowly varying functions of E and are regarded as constant in this paper. Thus, the boundary conditions at $r=r_0$ are met by each state Ψ_α irrespective of its energy. However, the boundary conditions at $r=\infty$ differ in continuum and discrete states. They are met by considering not just the eigenfunctions Ψ_α but superpositions

$$\Psi=\sum_\alpha \Psi_\alpha A_\alpha=\sum_i \Phi_i [f(\nu_i, r)\sum_\alpha U_{i\alpha}\cos\pi\mu_\alpha A_\alpha - g(\nu_i,r)\sum_\alpha U_{i\alpha}\sin\pi\mu_\alpha A_\alpha], \quad r>r_0 \quad (2.17)$$

with suitable coefficients A_α. The main condition on discrete states, that $f(\nu_i, r)$ and $g(\nu_i, r)$ remain finite at $r=\infty$ for each "closed channel"—i.e., for real values of ν_i—leads to the condition analogous to (2.8) [Eq. (28) of FH]

$$\sum_\alpha U_{i\alpha}\sin\pi(\nu_i+\mu_\alpha)A_\alpha=0 \quad (i=1,\ldots 5) . \quad (2.18)$$

The aim of this paper is to determine the parameters μ_α, D_α, and part of $U_{i\alpha}$ by fitting all available data on the absorption spectrum. There are five μ_α's, five D_α's, and ten independent elements of the 5×5 orthogonal matrix $U_{i\alpha}$. From this point of view, these parameters should be calculated by solving the Schrödinger equation for $r<r_0$ *only*, that is, with boundary conditions at $r=r_0$ instead of $r\to\infty$ and thus without distinguishing between discrete and continuum states. In the original QDT,[2] and in the early stages of this work,[4] no reference was made to the eigenstates Ψ_α but the observable spectrum was related to the nondiagonal reaction matrix $R_{ij}=-i[(S-1)/(S+1)]_{ij}$. The knowledge of the matrices R_{ij} or S_{ij} is equivalent to that of the matrix $U_{i\alpha}$ and eigenphase shift $\pi\mu_\alpha$ only if one actually diagonalizes S or R. By knowing the $U_{i\alpha}$ explicitly one finds the coupling of electron orbits and spins in the state Ψ_α; this information is complemented by the determination of the D_α. Since the interaction between the excited electron and the $(5p^5)$ core of Xe^+ is strong for $r\leq r_0$, it has been surmised[14] that the states Ψ_α would be LS coupled, with the classifications $[(5p^5)d]^1P_1$, $^3P_1$, $^3D_1$, and $[(5p^5)s]^1P_1$, $^3P_1$. If so, the dipole moment D_α should vanish for the three transitions to triplet Ψ_α. It will be shown that the experimental data verify this speculation only in part.

Section III develops formulas for energy levels, intensity distributions and other characteristics of the absorption spectrum as functions of the parameters $U_{i\alpha}$, μ_α, and D_α. Subsequent sections describe the determination of these parameters by fitting of experimental data.

III. ANALYTICAL TREATMENT

A. Discrete Spectrum

When the total energy E of the system falls below $I_{3/2}$, all channels are closed. To determine the discrete energy levels and their eigenfunctions we solve the system of five equations (2.18). To begin with, (2.18) is reduced to a system of two equations with two unknowns B_4 and B_5 by the substitution

$$A_\alpha=\frac{1}{\sin\pi(\nu_{3/2}+\mu_\alpha)}\sum_{j=4}^{5} U^\dagger_{\alpha j}B_j , \quad (3.1)$$

which satisfies three equations of (2.18), those with $i=1, 2, 3$. The remaining equations with $i=4$ and 5 are

$$\sum_{j=4}^{5}\left(\sum_{\alpha=1}^{5} U_{i\alpha}\frac{\sin\pi(\nu_{1/2}+\mu_\alpha)}{\sin\pi(\nu_{3/2}+\mu_\alpha)}U^\dagger_{\alpha j}\right)B_j=0 . \quad (3.2)$$

Alternatively, adding and subtracting $\pi\nu_{3/2}$ in the argument of $\sin\pi(\nu_{1/2}+\mu_\alpha)$ gives upon expansion

$$\sum_{j=4}^{5}[\cot\pi(\nu_{1/2}-\nu_{3/2})\delta_{ij}+M_{ij}(\nu_{3/2})]B_j=0 \quad (i=4, 5) , \quad (3.2')$$

where

$$M_{ij}=\sum_{\alpha=1}^{5} U_{i\alpha}\cot\pi(\nu_{3/2}+\mu_\alpha)U^\dagger_{\alpha j} . \quad (3.3)$$

The system (3.2) has nontrivial solutions when

$$F(\nu_{1/2}, \nu_{3/2})\equiv\det|\cot\pi(\nu_{1/2}-\nu_{3/2})\delta_{ij}+M_{ij}|=0 \quad (i, j=4, 5)$$

or

$$F(\nu_{1/2}, \nu_{3/2})=\cot^2\pi(\nu_{1/2}-\nu_{3/2})+(M_{44}+M_{55})\times\cot\pi(\nu_{1/2}-\nu_{3/2})+(M_{44}M_{55}-M_{45}M_{54})=0 . \quad (3.4)$$

This equation determines $\nu_{1/2}$ as a function of $\nu_{3/2}$ and plays a major role in the fitting procedure of this paper. The discrete *energy levels are given* by pairs of values of $\nu_{1/2}$ and $\nu_{3/2}$ which satisfy (2.10) and (3.4) simultaneously. A graphical procedure for the solution of these simultaneous relationships has been described in FH and in LF and is illustrated in Fig. 2.

Concerning the eigenfunctions, note initially that the system (2.18) has the special solution

$$A_\alpha=\delta_{\alpha\alpha'} \quad \text{when} \begin{cases}\nu_{3/2}=n_{3/2}-\mu_{\alpha'} , \\ \nu_{1/2}=n_{1/2}-\mu_{\alpha'} , \end{cases} \quad (3.5)$$

where $n_{3/2}$ and $n_{1/2}$ are any two integers and α' takes any value 1, 2, ... 5. According to these results the wave function Ψ reduces to $\Psi_{\alpha'}$, that is, the eigenstate of the complete collision problem is also the close-coupling eigenstate α'. As we shall see, some of the observed levels of Xe have values of $\nu_{3/2}$ and $\nu_{1/2}$ that fulfill (3.5) approximately; the wave functions of such levels are approximately close-coupling eigenstates of the $e+Xe^+$ collision

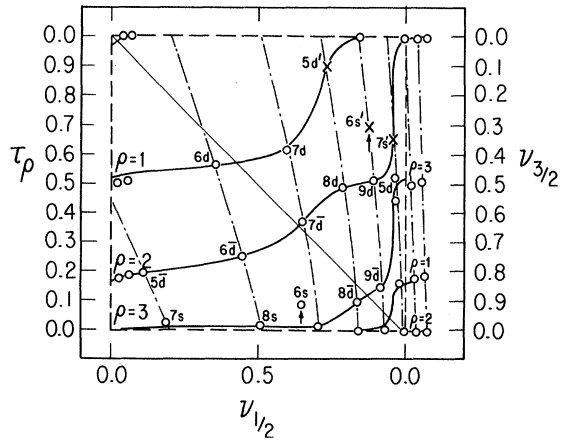

FIG. 2. Plot of $\nu_{3/2}$ or τ_ρ vs $\nu_{1/2}$. Open circles (○) and crosses (×) are level positions from Table II. Solid curves are Eq. (3.4), $F=0$, with parameters listed in Table I. Index ρ is labeled on each branch of the curve corresponding to one of the eigenphases $\pi\tau_\rho$. The diagonal line represents the equation $-\nu_{3/2}+\nu_{1/2}=0$. The function $-\nu_{3/2}(\nu_{1/2})$ defined by Eq. (4.1) is represented by dot-dashed lines. Some points are marked (†) to show departure from the $F=0$ curves.

complex. Graphically, these levels will lie near the diagonal $\nu_{3/2}-\nu_{1/2}=0$ (mod 1) on a $(\nu_{3/2}, \nu_{1/2})$ plot for discrete levels as suggested in LF and FH. The immediate result of the observation of levels which fulfill (3.5) is the determination of an eigenphase shift $\pi\mu_\alpha$ and the measurement of the relevant D_α from the experimental oscillator strength, as will be detailed in Secs. IV and VI.

Note also that (3.4) depends only on the following combinations of the elements of the transformation matrix $U_{i\alpha}$, which are invariant under orthogonal transformation of the two channels $i=4$, 5:

$$M_{44}+M_{55}=\sum_\alpha (U_{4\alpha}^2+U_{5\alpha}^2)\cot\pi(\nu_{3/2}+\mu_\alpha)\ , \tag{3.6}$$

$$M_{44}M_{55}-M_{45}^2=\sum_{\alpha\beta}(U_{4\alpha}U_{5\beta}-U_{5\alpha}U_{4\beta})^2 \times\cot\pi(\nu_{3/2}+\mu_\alpha)\cot\pi(\nu_{3/2}+\mu_\beta)\ . \tag{3.7}$$

Therefore, experimental data on the energy levels cannot by themselves determine the individual matrix elements $U_{4\alpha}$ and $U_{5\alpha}$, but only those invariant combinations which appear in (3.6) and (3.7). We emphasize that the invariant combinations

$$Q_{\alpha\beta}\equiv U_{4\alpha}U_{4\beta}+U_{5\alpha}U_{5\beta} \tag{3.8}$$

represent the matrix elements of a projection operator Q, with the properties

$$(Q^2)_{\alpha\beta}=\sum_\gamma Q_{\alpha\gamma}Q_{\gamma\beta}=Q_{\alpha\beta}\ ,\qquad \mathrm{Tr}Q=\sum_\alpha Q_{\alpha\alpha}=2\ . \tag{3.9}$$

The diagonal matrix element $Q_{\alpha\alpha}$ represents the squared projection of the eigenstate Ψ_α on the two-channel space $i=4$, 5 where Xe^+ is in the $^2P_{1/2}$ state. We stress that the data to be fitted in Secs. V and VI depend only on the subdivision of the dissociation channels into the groups, i.e., $i=1$, 2, 3 and $i=4$, 5, pertaining to different thresholds. Therefore fitting these data could not possibly determine the $U_{i\alpha}$ uniquely, but only the $Q_{\alpha\beta}$; experiments that distinguish between $i=1$, 2, 3 or between $i=4$ and 5 are necessary to get the full $U_{i\alpha}$.

It was found convenient to represent the solution of the homogeneous system (3.2′) in the form

$$B_5=h_{54}B_4\ , \tag{3.10}$$

where the ratio

$$h_{54}(\nu_{1/2},\ \nu_{3/2})=\frac{-M_{54}}{\cot\pi(\nu_{1/2}-\nu_{3/2})+M_{55}} \tag{3.11}$$

is obtained from (3.2′) with $i=5$ and where the value of $\nu_{1/2}-\nu_{3/2}$ must satisfy (3.4). The value of B_4 may be regarded as a normalization constant which cancels out in the calculation of oscillator strengths and of other observable parameters.

Consider now the nth solution $(\nu_{1/2,n},\ \nu_{3/2,n})$ of the simultaneous equations (2.10) and (3.4). To this pair of values of $\nu_{1/2}$ and $\nu_{3/2}$ corresponds an absorption line whose oscillator strength is given by a formula analogous to (2.9),

$$f_n=2(E_n-E_0)\left|\sum_\alpha D_\alpha A_\alpha^{(n)}\right|^2/\int|\Psi_n|^2d\tau\ , \tag{3.12}$$

where $A_\alpha^{(n)}$ is given by (3.1) and $\int|\Psi_n|^2d\tau$ is a normalization integral which reduces to ν_n^3 for a single channel. The normalization integral is worked out using the representation (2.17) of the wave function Ψ for $r>r_0$ and adapting the method in Sec. VI B of FH. The resulting equation, analogous to (57) of FH, is

$$\int|\Psi_n|^2d\tau=\left(\frac{d\nu_{3/2}}{dE}\right)_n\sum_{i=1}^{3}\left(\sum_\alpha U_{i\alpha}\cos\pi(\nu_{3/2,n}+\mu_\alpha)A_\alpha^{(n)}\right)^2 +\left(\frac{d\nu_{1/2}}{dE}\right)_n\sum_{i=4}^{5}\left(\sum_\alpha U_{i\alpha}\cos\pi(\nu_{1/2,n}+\mu_\alpha)A_\alpha^{(n)}\right)^2\ , \tag{3.13}$$

where

$$\left(\frac{d\nu_{3/2}}{dE}\right)_n=\nu_{3/2,n}^3\ ,\qquad \left(\frac{d\nu_{1/2}}{dE}\right)_n=\nu_{1/2,n}^3 \tag{3.13′}$$

according to (2.10). Substitution of (3.1) and (3.10) gives

$$\sum_\alpha D_\alpha A_\alpha^{(n)}=\left(\sum_\alpha D_\alpha\frac{1}{\sin\pi(\nu_{3/2,n}+\mu_\alpha)} \times[U_{\alpha4}^\dagger+U_{\alpha5}^\dagger h_{54}(\nu_{1/2,n},\ \nu_{3/2,n})]\right)B_4^{(n)}\ . \tag{3.14}$$

The coefficients of $\nu_{3/2,n}^3$ and $\nu_{1/2,n}^3$ in (3.13) are proportional, respectively, to the squared projections of Ψ_n on the channels converging to the limit

$I_{3/2}$ and $I_{1/2}$, i.e., on the channels with Xe^+ in the states $^2P_{3/2}$ and $^2P_{1/2}$. The coefficient of $\nu_{3/2,n}^3$ is calculated by introducing the projection matrix complementary to $Q_{\alpha\beta}$,

$$P_{\alpha\beta}=\sum_{i=1}^{3} U_{\alpha i}^{\dagger} U_{i\beta}=\delta_{\alpha\beta}-Q_{\alpha\beta}\ , \tag{3.15}$$

and the 2×2 symmetric matrix

$$N_{ij}(\nu_{3/2})=\sum_{\alpha,\beta} U_{i\alpha}\cot\pi(\nu_{3/2}+\mu_\alpha)P_{\alpha\beta}\cot\pi(\nu_{3/2}+\mu_\beta)U_{\beta j}^{\dagger}$$

$$(i,\ j=4,\ 5)\ . \tag{3.16}$$

Substitution of (3.1) and (3.10) into the coefficient of $\nu_{3/2n}^3$ in (3.13) yields

$$\sum_{i=1}^{3}\left(\sum_{\alpha} U_{i\alpha}\cos\pi(\nu_{3/2,n}+\mu_\alpha)A_\alpha^{(n)}\right)^2=\sum_{i,j=4}^{5} B_i^{(n)}N_{ij}(\nu_{3/2,n})B_j^{(n)}$$

$$=[N_{44}(\nu_{3/2,n})+2N_{45}(\nu_{3/2,n})\,h_{54}(\nu_{1/2,n},\ \nu_{3/2,n})+N_{55}(\nu_{3/2,n})h_{54}^2(\nu_{1/2,n},\ \nu_{3/2,n})]B_4^{(n)2}\equiv G_{3/2,n}B_4^{(n)2}\ . \tag{3.17a}$$

The coefficient of $\nu_{1/2,\,n}^3$ is simplified by using (3.2′):

$$\sum_{i=4}^{5}\left(\sum_{\alpha} U_{i\alpha}\cos\pi(\nu_{1/2,n}+\mu_\alpha)A_\alpha^{(n)}\right)^2$$

$$=\sum_{i=4}^{5}\left(\sum_{\alpha} U_{i\alpha}[\cos\pi(\nu_{1/2,n}-\nu_{3/2,n})\cot\pi(\nu_{3/2,n}+\mu_\alpha)-\sin\pi(\nu_{1/2,n}-\nu_{3/2,n})]\sum_{j} U_{\alpha j}^{\dagger}B_j^{(n)}\right)^2$$

$$=\frac{B_4^{(n)2}+B_5^{(n)2}}{\sin^2\pi(\nu_{1/2,n}-\nu_{3/2,n})}=\frac{1+h_{54}^2(\nu_{1/2,n},\ \nu_{3/2,n})}{\sin^2\pi(\nu_{1/2,n}-\nu_{3/2,n})}\,B_4^{(n)2}\equiv G_{1/2,n}B_4^{(n)2}\ . \tag{3.17b}$$

Substitution of these results reduces (3.12) to

$$f_n=2(E_n-E_0)\left(\sum_{\alpha} D_\alpha\frac{1}{\sin\pi(\nu_{3/2,n}+\mu_\alpha)}[U_{\alpha 4}^{\dagger}+U_{\alpha 5}^{\dagger}h_{54}(\nu_{1/2,n},\ \nu_{3/2,n})]\right)^2\Big/(\nu_{3/2,n}^3\,G_{3/2,n}+\nu_{1/2,n}^3\,G_{1/2,n})\ . \tag{3.18}$$

[The symbols $G_{3/2,n}$ and $G_{1/2,n}$ have been introduced in (3.17) to indicate the squared projections of Ψ_n on the channels with Xe^+ in the states $^2P_{3/2}$ and $^2P_{1/2}$.]

The special solution (3.5) arises in the limit where $\sin\pi(\nu_{1/2,n}+\mu_\alpha)$ and $\sin\pi(\nu_{3/2,n}+\mu_\alpha)$ vanish. In this limit (3.18) reduces to

$$\lim_{\substack{\nu_{3/2}\to -n-\mu_\alpha\\ \nu_{1/2}\to -n-\mu_\alpha}} f_n=2(E_n-E_0)\frac{|D_\alpha|^2}{\nu_{3/2,n}^3\,P_{\alpha\alpha}+\nu_{1/2,n}^3\,Q_{\alpha\alpha}}\ . \tag{3.19}$$

B. Auto-Ionization Spectrum

In the spectral range $I_{3/2}<E<I_{1/2}$ the parameter $\nu_{3/2}=i/k_{3/2}$ is imaginary while $\nu_{1/2}$ remains real. The condition that the closed-channel wave functions $f(\nu_{1/2},\ r)$ and $g(\nu_{1/2},\ r)$ remain finite at $r\to\infty$ yields only two of the five Eqs. (2.18), namely, those with $i=4,\ 5$. However, one recovers the other three Eqs. (2.18) in a modified form by introducing a boundary condition for the open channels, $i=1,\ 2,\ 3$.

We seek wave functions Ψ which behave for large r as collision eigenfunctions of the three channels that are actually open. There shall be three such eigenstates which we call Ψ_ρ, with $\rho=1,\ 2,\ 3$ (see Fig. 1). Recall that when all channels are open the close-coupling eigenfunctions Ψ_α are obtained from (2.12) by taking all pairs of coefficients $(c_i,\ d_i)$ in the ratio $d_i/c_i=\tan\pi\mu_\alpha$. To obtain a wave function Ψ_ρ from (2.17) we set the three pairs of coefficients with $i=1,\ 2,\ 3$ in a fixed ratio $\tan\pi\tau_\rho$,

$$\textstyle\sum_\alpha U_{i\alpha}\sin\pi\mu_\alpha A_\alpha\Big/\sum_\alpha U_{i\alpha}\cos\pi\mu_\alpha A_\alpha=\tan\pi\tau_\rho\ ,$$

$$i=1,\ 2,\ 3\ . \tag{3.20}$$

More specifically we set

$$\left.\begin{aligned}\textstyle\sum_\alpha U_{i\alpha}\cos\pi\mu_\alpha A_\alpha&=T_{i\rho}\cos\pi\tau_\rho\ ,\\ \textstyle\sum_\alpha U_{i\alpha}\sin\pi\mu_\alpha A_\alpha&=T_{i\rho}\sin\pi\tau_\rho\ ,\end{aligned}\right\}\quad i=1,\ 2,\ 3 \tag{3.21}$$

where each coefficient $T_{i\rho}$ represents the probability amplitude of the ith channel wave function in the state Ψ_ρ and $\pi\tau_\rho$ represents the eigenphase shift of the collision eigenfunction Ψ_ρ. The wave function of the eigenstate ρ is then represented by a superposition of standing waves of the open channels $i=1,\ 2,\ 3$ for large distance r and also, at somewhat smaller distances, by exponentially damped waves in the closed channels, $i=4,\ 5$:

$$\Psi_\rho\underset{r\to\infty}{\longrightarrow}\sum_{i=1}^{3}\Phi_i\left(\frac{2}{\pi k_{3/2}}\right)^{1/2}\sin\left[k_{3/2}r-\tfrac{1}{2}\pi l_i+\frac{1}{k_{3/2}}\ln(2k_{3/2}r)\right.$$

$$\left.+\arg\Gamma\left(l+1-\frac{i}{k_{3/2}}\right)+\pi\tau_\rho\right]T_{i\rho}$$

$$-\sum_{i=4}^{5}\Phi_i v(\nu_{1/2},\ r)\sum_{\alpha} U_{i\alpha}\cos\pi(\nu_{1/2}+\mu_\alpha)A_\alpha\ . \tag{3.22}$$

To determine the A_α we eliminate $T_{i\rho}$ from the Eq. (3.21) and find

$$\sum_\alpha U_{i\alpha} \sin\pi(\mu_\alpha - \tau_\rho) A_\alpha = 0 \ , \quad i = 1, 2, 3 \ . \quad (3.23)$$

An essential point of our treatment is that these equations differ from the first three Eqs. (2.18) merely by the substitution

$$\nu_{3/2} \longrightarrow -\tau_\rho \ (\text{mod } 1) \ . \quad (3.24)$$

This means that the parameter $\nu_{3/2}$ of each level of the discrete spectrum can be represented in the form $\nu_{3/2} = n - \tau_\rho$, where τ_ρ is an effective quantum defect and $\pi\tau_\rho$ represents the phase shift of the collision eigenfunction Ψ_ρ for $I_{1/2} > E > I_{3/2}$. Thus we have established here, as in FH, a correspondence between bound-state levels and continuum eigenstates, which is analogous to that for single-channel problems.

The quantum defect τ_ρ may be regarded as an eigenvalue of the system of equations for the A_α. The secular equation for this system has the form (3.4) with $\nu_{3/2}$ replaced by $-\tau_\rho$. Equation (3.4) is derived from (3.1) and (2.18) as a quadratic equation in $\cot\pi(\nu_{1/2} - \nu_{3/2})$ with coefficients that are functions of $\nu_{3/2}$. Alternatively, one can derive a relationship to yield $\nu_{3/2} = -\tau_\rho$ (mod 1) as a function of $\nu_{1/2}$ such that there are three roots τ_ρ for each value of $\nu_{1/2}$. Whereas quantum defects and phase shifts are usually slowly varying functions of energy, the influence of the "closed channels" $i = 4, 5$ causes the τ_ρ to vary sharply as periodic functions of $\nu_{1/2}$ as will be demonstrated in the following sections.

The coefficients A_α are similarly given by (3.1) and (3.10) with $\nu_{3/2}$ replaced by $-\tau_\rho$. The density of oscillator strength in the auto-ionization spectrum is given by a formula analogous to (2.5) and (3.18). It results as the sum of contributions corresponding to photo-ionization into the three eigenchannels ρ, namely,

$$\frac{df}{dE} = \sum_\rho \frac{df^{(\rho)}}{dE} = 2(E - E_0) \sum_\rho \Big| \sum_\alpha D_\alpha A_\alpha(\tau_\rho) \Big|^2 \Big/ \int dE' \int \Psi^\dagger_{E_\rho} \Psi_{E'_\rho} d\tau \ . \quad (3.25)$$

Here the expression in the numerator is obtained from (3.14) with the substitution $\nu_{3/2} \rightarrow -\tau_\rho$ and the denominator is evaluated in accordance with (3.22) and (3.17a) to give

$$\int dE' \int \Psi^\dagger_{E_\rho} \Psi_{E'_\rho} d\tau = \Big(\int dE' \, \delta(E - E') \Big) \sum_{i=1}^{3} T^2_{i\rho}$$
$$= \sum_{i=1}^{3} \Big(\sum_\alpha U_{i\alpha} \cos\pi(\mu_\alpha - \tau_\rho) A^{(\rho)}_\alpha \Big)^2$$
$$= G_{3/2}(\nu_{1/2}, -\tau_\rho) B_4^{(\rho)2} \ . \quad (3.26)$$

Thus (3.25) becomes

$$\frac{df}{dE} = \sum_\rho \frac{df^{(\rho)}}{dE} = 2(E - E_0) \sum_\rho \Big(\sum_\alpha D_\alpha \frac{1}{\sin\pi(\mu_\alpha - \tau_\rho)} [U^\dagger_{\alpha 4} + U^\dagger_{\alpha 5} h_{54}(\nu_{1/2}, -\tau_\rho)] \Big)^2 \Big/ G_{3/2}(\nu_{1/2}, -\tau_\rho) \ . \quad (3.27)$$

Notice that $T_{i\rho}$ coincides with $\sum_\alpha U_{i\alpha} \cos\pi(\mu_\alpha - \tau_\rho) A^{(\rho)}_\alpha$ for $i = 1, 2, 3$ and that $\sum_{i=1}^3 T_{i\rho}^2$ coincides with the squared projection $G_{3/2}(\nu_{1/2}, -\tau_\rho)$ of $\Psi^{(\rho)}$ on the channels with Xe^+ in the $^2P_{3/2}$ state.

C. Open Continuum

When the total energy E exceeds $I_{1/2}$, all the channels are open. The total oscillator strength for photoabsorption in the continuum is given by (2.5) with $|D|^2$ replaced by $\sum_\alpha |D_\alpha|^2$. The probability of ionization into a specific close-coupling eigenstate α is not observed by a specific experiment. We are interested here in the ratio of probabilities of photo-ionization into any of the three channels with $i = 1, 2, 3$ and into any of the other two channels $i = 4, 5$, because this ratio equals the intensity ratio of two photoelectron groups with energies $\frac{1}{2}k_{3/2}^2$ and $\frac{1}{2}k_{1/2}^2$.

To obtain this ratio we calculate first the probability of ejection of a photoelectron into each specific channel $\bar{i}$. The final state of this process is represented, for large r, by a wave function $\Psi^{(\bar{i}-)}$. This wave function is obtained from (2.17) by choosing coefficients $A_\alpha = A^{(\bar{i}-)}_\alpha$ such that the amplitude of the outgoing wave vanishes in all channels $i \neq \bar{i}$. As detailed in Sec. IV of FH, the desired coefficients are

$$A^{(\bar{i}-)}_\alpha = e^{-i\pi\mu_\alpha} U^\dagger_{\alpha\bar{i}} \ . \quad (3.28)$$

The result is verified by substituting in (2.17) the large r forms of

$$f(\nu_i, r) \sim (2/k_i\pi)^{1/2} \sin(k_i r + \cdots)$$

and

$$g(\nu_i, r) \sim -(2/k_i\pi)^{1/2} \cos(k_i r + \cdots)$$

together with the coefficients (3.28).

The oscillator strength for photoemission of electrons with kinetic energy $\frac{1}{2}k_{3/2}^2$ is then

$$\frac{df^{(3/2)}}{dE} = 2(E - E_0) \sum_{i=1}^{3} \Big| \sum_\alpha D_\alpha e^{-i\pi\mu_\alpha} U^\dagger_{\alpha i} \Big|^2$$
$$= 2(E - E_0) \sum_{\alpha,\beta=1}^{5} P_{\alpha\beta} \cos\pi(\mu_\alpha - \mu_\beta) D_\alpha D_\beta \ , \quad (3.29)$$

where $P_{\alpha\beta}$ is the projection operator matrix (3.15). Similarly, the oscillator strength for photoemission

of electrons with kinetic energy $\frac{1}{2}k_{1/2}^2$ is

$$\frac{df^{(1/2)}}{dE} = 2(E-E_0)\sum_{\alpha,\beta=1}^{5} Q_{\alpha\beta}\cos\pi(\mu_\alpha-\mu_\beta)D_\alpha D_\beta\ , \quad (3.30)$$

with $Q_{\alpha\beta}$ given by (3.8). The branching ratio is then

$$\frac{df^{(3/2)}}{dE}\Big/\frac{df^{(1/2)}}{dE} = \sum_{\alpha\beta} P_{\alpha\beta}\cos\pi(\mu_\alpha-\mu_\beta)D_\alpha D_\beta \Big/ \sum_{\alpha\beta} Q_{\alpha\beta}\cos\pi(\mu_\alpha-\mu_\beta)D_\alpha D_\beta\ . \quad (3.31)$$

Notice that this ratio depends on the matrices $P_{\alpha\beta}$ and $Q_{\alpha\beta}=\delta_{\alpha\beta}-P_{\alpha\beta}$, which are combinations of matrix elements $U_{i\alpha}$. Therefore its experimental measurement gives only information on $P_{\alpha\beta}$ and $Q_{\alpha\beta}$ but not on the individual elements $U_{i\alpha}$. The same holds for the observable quantities obtained above in A and B. On the other hand, evidence on the $U_{i\alpha}$ could be obtained by observing the angular distribution of photoelectrons which depends on the wave functions Φ_i of individual channels.

In summary we may say that this section has formulated the relationships between the eigenstates α and the various dissociation channels which are indicated in the diagram in Fig. 1.

IV. GRAPHICAL REPRESENTATION

In our method the qualitative analysis of the spectrum centers on the relation between $\nu_{1/2}$ and $\nu_{3/2}$ established by Eq. (3.4), $F(\nu_{1/2}, \nu_{3/2})=0$. This relationship is represented graphically in Fig. 2 (which is essentially the same as Fig. 1 of LF). [Note that the scale of $\nu_{3/2}$ increases downwards while that of the quantum defect $\tau_\rho=-\nu_{3/2}$ (mod 1) increases upward in the figure; all scales are mod 1]. For each discrete energy level of the experimental spectrum a pair of values $(\nu_{1/2}, \nu_{3/2})$ is determined from (2.10) and is represented by one point in Fig. 2. Note that each point must lie at the intersection of the curves obtained from (a) the relation

$$\nu_{3/2}^{\,2}=\nu_{1/2}^{\,2}[1-2(I_{1/2}-I_{3/2})\nu_{1/2}^{\,2}]^{-1}\ , \quad (4.1)$$

derived from (2.10), and (b) $F(\nu_{1/2}, \nu_{3/2})=0$. The full curve in Fig. 2 represents the analytic relation $F(\nu_{1/2}, \nu_{3/2})=0$, whose parameters have been determined to fit the experimental data as detailed in Sec. V below. Since $F(\nu_{1/2}, \nu_{3/2})$ consists of cotangent functions of $\pi\nu_{1/2}$ and $\pi\nu_{3/2}$, it is a periodic function of $\nu_{1/2}$ and $\nu_{3/2}$ with period 1; therefore it is sufficient to plot $F=0$ on a 1×1 square of the range of these variables, i.e., mod 1 in both $\nu_{1/2}$ and $\nu_{3/2}$.

Two outstanding features of Fig. 2 help to determine the parameters of the theory:

(i) The special solution (3.5) implies that $F(-\mu_\alpha, -\mu_\alpha)=0$. As has been explained, the wave function Ψ of the atom coincides with the close-coupling eigenstate α when (3.5) is satisfied. The points of coordinates $(-\mu_\alpha, -\mu_\alpha)$ are accordingly the intersections of $F(\nu_{1/2}, \nu_{3/2})=0$ with the diagonal $\nu_{3/2}=\nu_{1/2}$. Thus the eigenphase shift $\pi\mu_\alpha$ can be determined by interpolation when no level fulfills (3.5) closely but two levels are represented on the $(\nu_{1/2}, \nu_{3/2})$ plot by points which straddle the diagonal $\nu_{3/2}=\nu_{1/2}$.

(ii) The slope of the curve $F(\nu_{1/2}, \nu_{3/2})=0$ equals

$$Q_{\alpha\alpha}/P_{\alpha\alpha}=Q_{\alpha\alpha}/(1-Q_{\alpha\alpha}) \quad (4.2)$$

at each of the intersection points of $F(\nu_{1/2}, \nu_{3/2})$ with the diagonal line $\nu_{1/2}=\nu_{3/2}$, i.e., at $(-\mu_\alpha, -\mu_\alpha)$. Therefore the diagonal elements of the projection operator P and Q can be approximately determined from a preliminary plot of $F=0$ obtained by interpolation through experimental points.

The representation (4.2) of the slope at $(-\mu_\alpha, -\mu_\alpha)$ is but a special case of a more general relation. The slope of the curve $F=0$ at any point is represented by

$$\frac{d(-\nu_{3/2})}{d\nu_{1/2}} = \frac{\partial F}{\partial\nu_{1/2}}\Big/\frac{\partial F}{\partial\nu_{3/2}} = \frac{G_{1/2}}{G_{3/2}}\ . \quad (4.3)$$

The numerator and denominator of this formula are the quantities proportional to the coefficients of $\nu_{1/2}^{\,3}$ and of $\nu_{3/2}^{\,3}$ in (3.13), respectively. As noted in Sec. III, these coefficients represent the squared overlap integrals of a state Ψ with the "Q" channels ($i=4, 5$) and "P" channels ($i=1, 2, 2$), respectively, and are therefore non-negative. Hence we have

$$\frac{d(-\nu_{3/2})}{d\nu_{1/2}} \geq 0\ ; \quad (4.4)$$

that is, the curve representing $F=0$ is a monotonically increasing function of $\nu_{1/2}$.

In its form (3.4), the equation $F(\nu_{1/2}, \nu_{3/2})=0$ is a quadratic equation in $\cot\pi(\nu_{1/2}-\nu_{3/2})$ with coefficients depending on $\nu_{3/2}$. Hence it has two roots $\nu_{1/2}$ for each given value of $\nu_{3/2}$. Likewise, an alternative form of (3.4) could be derived which yields three roots $\nu_{3/2}$ for each value of $\nu_{1/2}$. Hence any horizontal line in Fig. 2 intersects the curve $F(\nu_{1/2}, \nu_{3/2})=0$ twice and any vertical line intersects the curve three times. Since $F(\nu_{1/2}, \nu_{3/2})$ is a periodic function of both $\nu_{3/2}$ and $\nu_{1/2}$ each branch of the curve which exits from one margin of the basic unit square of the plot reappears at the corresponding point of the opposite margin. If one regards such corresponding points on opposite margins as the "same" point, all branches of the curve in the figure are seen to be parts of a single continuous curve.

In our example, the quantum defects of the three Rydberg series of Xe converging to the limit $I_{3/2}$ are perturbed by states from Rydberg series converging to the limit $I_{1/2}$, which are represented in Fig. 2 by the crosses $\times$. If one follows any one

branch of the curve, one sees that it makes two consecutive stepwise jumps before it emerges from the other end of the figure. In the scattering problem the sum of the phases of all open channels increases by π at each resonance; here the sum of the three τ_ρ values increases by unity. In all three regards, the behavior of the quantum defects of discrete spectral levels in Fig. 2 resembles that of scattering eigenphases near two adjacent resonances.

If all interactions between series were very weak, all unperturbed levels of the "perturbed" series would lie on flat portions of the curves and the levels of the "perturbing" series would lie on the sharp vertical portions of the curves; pairs of curves would nearly touch each other at the step corners. In Fig. 2 gaps of various magnitudes remain between branches of the curve which approach one another but fail to cross. The magnitude of the gaps at such avoided crossings gives a graphical indication of the strength of interactions.[4] In particular the branches of $F(\nu_{1/2}, \nu_{3/2}) = 0$ corresponding to levels labeled ns and ns' in Table II come fairly close to each other, namely, to within a distance of ~ 0.05.[15] On the other hand, the branches corresponding to d levels stay so much apart that one can hardly identify regions of avoided crossing. The avoided crossings of d and s branches have gaps of the order of 0.05 indicating a fairly weak s-d interaction.

In the auto-ionization region of the spectrum, the ordinates of the curves $F(\nu_{1/2}, \nu_{3/2}) = 0$ represent the eigenphases (in units of π) of the scattering matrix for the three-channel collision $e + \mathrm{Xe}^+(^2P_{3/2})$. Each branch of the curve in Fig. 2 is labeled by the index ρ corresponding to one of the eigenphases $\pi\tau_\rho$. The two stepwise rises of each branch correspond to the characteristic rise of a phase shift at resonances.[16] The present treatment is equally applicable whether the resonances are sharp, as assumed for the isolated resonances of Ref. 16, or so wide as to barely permit the identification of overlapping resonances.[17] The gap at each avoided crossing of the ρth branch now measures the partial width for decay of the resonance into the continuum state Ψ_ρ.

V. PARAMETER FITTING OF $F(\nu_{1/2}, \nu_{3/2}) = 0$

The function $F(\nu_{1/2}, \nu_{3/2})$ defined in (3.4) depends on the five parameters μ_α and on the ten parameters $U_{4\alpha}$ and $U_{5\alpha}$, though the latter are not independent as noted before. These parameters will now be determined such that the plot of $F = 0$ in Fig. 2 passes as close as possible to the points that represent the experimentally observed discrete levels. The values of the parameters finally adopted by trial and error are given in Table I. The procedure followed in obtaining the parameters is described briefly and then the interpretation of the results is discussed.

The values of μ_α can be read off initially from Fig. 2, to ≈ 0.01 accuracy:

$$\begin{aligned} \alpha &= \quad 1 \quad\; 2 \quad\; 3 \quad\; 4 \quad\; 5 \quad , \\ \mu_\alpha &= 0.57 \;\; 0.36 \;\; 0.13 \;\; 0.05 \;\; 0.005 \; . \end{aligned} \tag{5.1}$$

The same holds, to somewhat lower accuracy, for $Q_{\alpha\alpha}$ by measuring the slope of $F = 0$ at $\nu_{1/2} = \nu_{3/2} = -\mu_\alpha$ (mod 1) and applying (4.2). Note from the definition (3.8) of $Q_{\alpha\beta}$ that

$$Q_{\alpha\alpha} = U_{4\alpha}^2 + U_{5\alpha}^2 \; . \tag{5.2}$$

The condition

$$\sum_{\alpha=1}^{5} Q_{\alpha\alpha} = 2 \tag{5.3}$$

arising from the orthonormality of $U_{i\alpha}$ imposes a consistency check on the values of $Q_{\alpha\alpha}$ obtained from the curves of Fig. 2. The additional conditions of orthonormality

$$\textstyle\sum_\alpha U_{4\alpha}^2 = \sum_\alpha U_{5\alpha}^2 = 1 \; , \quad \sum_\alpha U_{4\alpha} U_{5\alpha} = 0 \tag{5.4}$$

reduce the number of independent parameters $U_{4\alpha}$ and $U_{5\alpha}$ to seven.

Preliminary fitting. A stepwise procedure was followed, utilizing the fact that the coupling between excited states with an s and with a d electron is rather weak, as mentioned in LF and in Sec. IV. Thus we assume that the five-channel problem separates into one two-channel problem with s-state excitation and one three-channel problem with d-state excitation. Under this assumption the consistency equation $F = 0$ factors out in the form

$$F \approx F_s(\nu_{1/2}, \nu_{3/2}) F_d(\nu_{1/2}, \nu_{3/2}) = 0 \; .$$

We assume more specifically that the excited electron has approximately d character in the eigenchannels $\alpha = 1, 2, 3$ and s character in $\alpha = 4, 5$. In view of the channel identification in Eq. (2.11), the above assumptions imply that all the matrix elements $U_{i\alpha}$ which connect states with s and d character are zero. One now sets $U_{4\alpha} = 0$ for $\alpha = 4, 5$ and $U_{5\alpha} = 0$ for $\alpha = 1, 2, 3$. [Remember that in solving the Eqs. (2.18) for $i = 1, 2, \ldots 5$, we made the substitution (3.1) which left us with a consistency equation (3.4) dependent only on $U_{i\alpha}$ for $i = 4, 5$.] From Eq. (3.8), the matrix $Q_{\alpha\beta}$ reduces to separate square blocks, with matrix elements $Q_{\alpha\beta} = 0$ for either ($\alpha = 1, 2, 3$; $\beta = 4, 5$) or ($\alpha = 4, 5$; $\beta = 1, 2, 3$). To distinguish the parameters evaluated with this approximation we write now $U_{d\alpha}$ in place of $U_{4\alpha}(\alpha = 1, 2, 3)$ and $U_{s\alpha}$ in place of $U_{5\alpha}(\alpha = 4, 5)$.

With this understanding the Eq. (3.4) ($F = 0$) splits now into two equations, one for d channels:

$$F_d(\nu_{3/2}, \nu_{1/2}) = \cot\pi(\nu_{1/2} - \nu_{3/2}) + M_{dd}$$

$$= \cot\pi(\nu_{1/2}-\nu_{3/2}) + \sum_{\alpha=1}^{3} U_{d\alpha}^2 \cot\pi(\nu_{3/2}+\mu_\alpha) \approx 0 \ , \quad (5.5)$$

and one for s channels:

$$F_s(\nu_{3/2},\ \nu_{1/2}) = \cot\pi(\nu_{1/2}-\nu_{3/2}) + M_{ss}$$

$$= \cot\pi(\nu_{1/2}-\nu_{3/2}) + \sum_{\alpha=4}^{5} U_{s\alpha}^2 \cot\pi(\nu_{3/2}+\mu_\alpha) \approx 0 \ , \quad (5.6)$$

since $M_{ds} = M_{sd} \approx 0$.

In both cases, the $U_{i\alpha}^2$'s ($i = d$ or s) are just the $Q_{\alpha\alpha}$ itself in the present approximation. Thus F_d and F_s depend on μ_α and $Q_{\alpha\alpha}$ only, both of which can approximately be read from Fig. 2.

The separate curves representing the equations $F_s = 0$ and $F_d = 0$ are plotted in Fig. 3. As expected, these curves show a fair fitting with the experimental points except in the limited regions where the "s" and "d" curves cross, since the avoided crossing shown in Fig. 2 results from the s-d interaction which we have disregarded.

Within the approximation of zero s-d coupling we can also test the further assumption that the close-coupling eigenstates have LS-coupling character. Specifically we test the following assignments:

$\alpha =$	1	2	3	4	5
μ_α(mod 1) =	0.57	0.36	0.13	0.05	0.005
assignment =	$(p^5d)\,^3P$	$(p^5d)\,^3D$	$(p^5d)\,^1P$	$(p^5s)\,^3P$	$(p^5s)\,^1P$

(5.7)

which was arrived at by the following reasoning:

(a) From Moore's table,[7] the s electrons have smaller quantum defects (mod 1) than the d electrons.

(b) By Hund's rule, within the set of d's and within the set of s's the triplets have lower energy and hence higher quantum defect than singlets.

(c) The relative assignment of $(p^5d)\,^3P$ and $(p^5d)\,^3D$ will be explained in the Appendix.

The assignment (5.7) defines the matrix elements $U_{d\alpha}$ and $U_{s\alpha}$ as recoupling coefficients of a $(LS|jj)$ transformation. We list here the values of the squared coefficients obtained theoretically as elements of the transformation matrix $(LS|jj)$ and compare them with the values $Q_{\alpha\alpha}$ derived from the plot of Fig. 3:

	U_{d1}^2	U_{d2}^2	U_{d3}^2	U_{s4}^2	U_{s5}^2
$(LS\|jj)^2$	$\frac{1}{6}$	$\frac{1}{2}$	$\frac{1}{3}$	$\frac{2}{3}$	$\frac{1}{3}$
$Q_{\alpha\alpha}$	0.14	0.48	0.38	0.82	0.18 .

(5.8)

The largest discrepancy in (5.8), for the s states, indicates that the coupling of the eigenstates $\alpha = 4$, 5 is intermediate between LS and jj, since jj coupling would give $U_{s4}^2 = 1$ and $U_{s5}^2 = 0$. This result of the analysis is discussed in Sec. VIII. The next largest discrepancy, between the values 0.38 and $\frac{1}{3}$ for U_{d3}^2, also appears experimentally significant and relates to the intensity of different photoelectron groups as will be discussed in Sec. VI. The remaining discrepancies between the elements $(LS|jj)^2$ (which are approximations to the $U_{d\alpha}^2$) and the $Q_{\alpha\alpha}$ are fairly small, showing fair agreement with the assumption that the close coupling eigenstates have LS-coupling character for the three d channels, $\alpha = 1$, 2, 3.

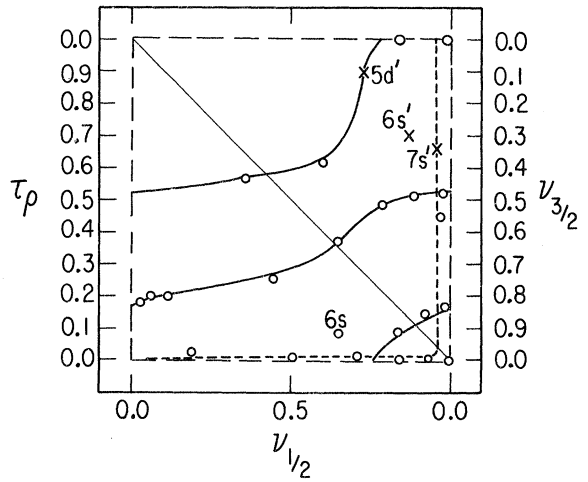

FIG. 3. Preliminary fitting of discrete levels. The full curve and dashed curve represent Eq. (5.5), $F_d = 0$, and (5.6), $F_s = 0$, respectively.

Further fitting. We proceed now to a final determination of coefficients $U_{4\alpha}$ and $U_{5\alpha}$, removing the restrictions $U_{d\alpha} = 0$ for $\alpha = 4$, 5 and $U_{s\alpha} = 0$ for $\alpha = 1$, 2, 3. However, as we do so the i channel previously designated as "4" or "d" no longer has purely d character and can no longer be identified with the channel defined as "4" in Eq. (2.11). Accordingly the modified $U_{d\alpha}$ will now be called $U_{\bar{4}\alpha}$ and similarly the $U_{s\alpha}$ will be called $U_{\bar{5}\alpha}$. Here $\bar{4}$ and $\bar{5}$ are channels identified, but not precisely, as being close to 4 and 5 as defined in (2.11).

To see the effect of s-d coupling we tentatively assign the small value 0.01 to all the squared matrix elements previously set to zero, $U_{\bar{4}4}^2$, $U_{\bar{4}5}^2$, $U_{\bar{5}1}^2$, $U_{\bar{5}2}^2$, and $U_{\bar{5}3}^2$. The restrictions previously adopted with regard to $Q_{\alpha\alpha}$, namely, that

$$\sum_{\alpha=1}^{3} Q_{\alpha\alpha} = \sum_{\alpha} U_{d\alpha}{}^2 = 1 \quad \text{and} \quad \sum_{\alpha=4} Q_{\alpha\alpha} = \sum_{\alpha} U_{s\alpha}^2 = 1$$

were also relaxed to the extent of 0.01, while (5.3) was of course enforced. The relative signs of the "small" $U_{\bar{4}\alpha}$ and $U_{\bar{5}\alpha}$ coefficients (of order 0.1) were chosen to yield an adequate fit to Fig. 2, using the orthonormality condition Eq. (5.4) to limit the number of signs. These coefficients influence the fitting through the matrix element $M_{\bar{4}\bar{5}} = \sum_\alpha U_{\bar{4}\alpha} U_{\bar{5}\alpha} \cot\pi$

$\times(\mu_\alpha+\nu_{3/2})$, which appears in Eq. (3.4) and represents the s-d interaction but vanishes in the approximation leading to (5.5) and (5.6). The "final" choice of parameters $U_{\bar{4}\alpha}$ and $U_{\bar{5}\alpha}$ is shown in Table I. Due to the indeterminacy of $U_{i\alpha}$, noted in Sec. III, this set was obtained by assuming the small $U_{\bar{4}\alpha}$'s and $U_{\bar{5}\alpha}$'s are equal to 0.1 and adjusting the large $U_{\bar{4}\alpha}$'s and $U_{\bar{5}\alpha}$'s with the understanding that the square of these matrix elements are close to the corresponding $Q_{\alpha\alpha}$'s, so that Eq. (5.4) is satisfied and so that one obtains a good fit to the experimental data.

For further analysis it is convenient to give the matrix $Q_{\alpha\beta}=U_{\bar{4}\alpha}U_{\bar{4}\beta}+U_{\bar{5}\alpha}U_{\bar{5}\beta}$ constructed with these parameters

$$\beta=\quad 1 \quad 2 \quad 3 \quad 4 \quad 5$$

$$(Q_{\alpha\beta})=\begin{vmatrix} 0.14 & 0.26 & 0.21 & -0.052 & -0.077 \\ & 0.49 & 0.41 & -0.017 & -0.11 \\ & & 0.38 & -0.15 & -0.019 \\ & & & 0.81 & 0.36 \\ & & & & 0.18 \end{vmatrix} . \tag{5.9}$$

As a consistency check, it was verified that the elements of this matrix satisfy Eq. (3.9), $Q_{\alpha\gamma}=\sum_\beta Q_{\alpha\beta}Q_{\beta\gamma}$, within 0.003.

VI. FITTING OF OSCILLATOR STRENGTH

In this section we fit initially the dipole strength parameters D_α in the oscillator strength formula (3.27) to reproduce the intensity profile in the auto-ionization spectrum measured by Huffman *et al.*[9] The ability of the formula to reproduce the experimental data serves as a first test of our formulation. A second and more stringent test is that Eq. (3.18) with the same parameters D_α should fit the discrete spectrum oscillator strength of Ref. 8. Finally, the same parameters will be entered in the branching ratio expression (3.31) to compare the results with the ratio measured by Samson and Cairns.[6]

Recall that all parameters are regarded in this paper as approximately independent of energy over the range of a few eV covered by our analysis. It might then be inconsistent to treat the factor $E-E_0$ of the oscillator strength as variable, since its variation should be of the same order as that of other parameters. Accordingly we replace the dipole element D_α by

$$\varphi_\alpha=[2(E-E_0)]^{1/2}D_\alpha \tag{6.1}$$

and adjust φ_α rather than D_α to fit experimental data.

A. Auto-Ionization Spectrum

The measurements of absorption coefficients, i.e., of oscillator strengths, in the auto-ionization spectrum do not separate out the contributions of photo-ionization to the three collision eigenchannels $\rho=1, 2, 3$. Therefore the quantity to be fitted is the total contribution

$$\frac{df}{dE}=\sum_{\rho=1}^{3}\frac{df^{(\rho)}}{dE} . \tag{6.2}$$

However, it is important for us to calculate the separate terms of (6.2) because it is these that also fit the oscillator strength of discrete lines. This analysis of the auto-ionization intensity as the sum of three terms differs substantially from that introduced by Fano[18] and carried out in detail by Comes and Sälzer.[19] The Fano approach represents the spectrum by interference of auto-ionization lines with a smooth background. The two approaches are actually equivalent.

Since the auto-ionization spectrum observed by Huffman is periodic in terms of the effective quantum number $\nu_{1/2}$ within the experimental error, we have fitted only the section between $\nu_{1/2}=3.55$, i.e., just above the $I_{3/2}$ threshold where accuracy is highest, and $\nu_{1/2}=4.55$. Figure 4 shows the final fitting that was achieved using the values of the parameters φ_α given in Table I. As elsewhere in this work, consistency with the rest of the treatment justified only a modest effort to obtain an accurate fit. Dashed curves in Fig. 4 represent the result of the preliminary fitting described below. Figure 5 shows the separate contributions of the

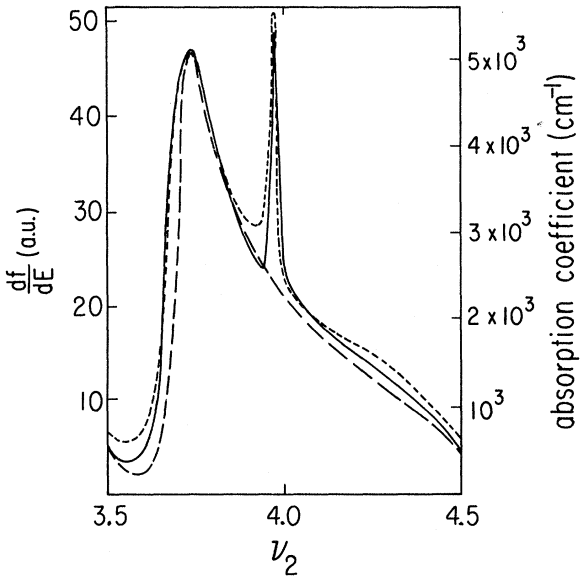

FIG. 4. Xenon auto-ionization profile between $\nu_{1/2}=3.55$ and 4.55. The full curve represents the measured profile by Huffman *et al.* (Ref. 9) plotted as function of $\nu_{1/2}$. The dashed curve is the one-channel fitting corresponding to Eq. (6.3a) with $\varphi_3\neq 0$ and $\varphi_1=\varphi_2=0$. The dotted curve represents the fitting of the intensity profile given by Eq. (3.27) with φ_α's listed in Table I.

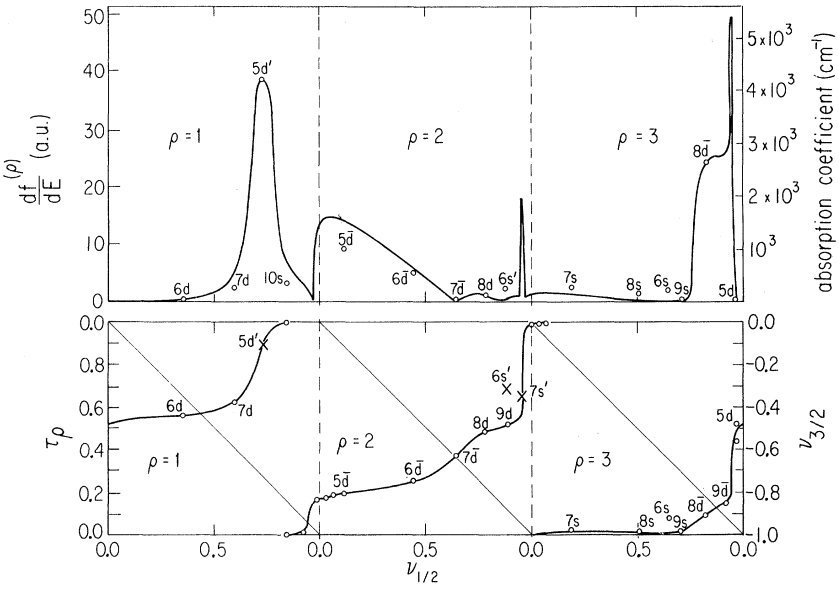

FIG. 5. Oscillator strengths of Xe in the discrete and auto-ionization region. The full curve in the upper portion of the figure shows the separate contribution of the oscillator strength $df^{(\rho)}/dE$ for photo-ionization into ρth collision. eigenstates of the auto-ionization region as function fo $\nu_{1/2}$ over three periods of $\nu_{1/2}$; each period corresponds to one of the three roots τ_ρ of the Eq. (3.4), $F(\nu_{1/2}, -\tau_\rho) = 0$. The corresponding root τ_ρ is plotted below the main graph for purposes of identification. The labeled open circles (ȯ) in the upper portion of the figure are the reduced discrete line intensities obtained by dividing the discrete oscillator strength f_n from Ref. 8 by the coefficient (6.5). No measured point has been omitted.

oscillator strength for photo-ionization into collision eigenstates of the auto-ionization region.

As in the fitting of discrete energy levels (Sec. V), we disregard initially the interaction of d and s channels, i.e., we set such matrix elements as $U_{4\alpha} \equiv U_{d\alpha}$ ($\alpha = 4, 5$) and $U_{5\alpha} \equiv U_{s\alpha}$ ($\alpha = 1, 2, 3$) to be zero. Under this approximation the expression (3.27) of $df^{(\rho)}/dE$ is replaced by the sum of two separate terms

$$\frac{df_d^{(\rho)}}{dE} \approx \left(\sum_{\alpha=1}^{3} \varphi_\alpha \frac{1}{\sin\pi(\mu_\alpha - \tau_\rho)} U_{\alpha d}^{\dagger} \right)^2 \Big/ N_{dd} \,, \quad (6.3a)$$

$$\frac{df_s^{(\rho)}}{dE} \approx \left(\sum_{\alpha=4}^{5} \varphi_\alpha \frac{1}{\sin\pi(\mu_\alpha - \tau_\rho)} U_{\alpha s}^{\dagger} \right)^2 \Big/ N_{ss} \,. \quad (6.3b)$$

A further simplification follows from the fact that the eigenstate $\alpha = 3$ was identified in Sec. V as approximately ^1P, while $\alpha = 1, 2$ were identified as approximately triplets. Under this assumption the oscillator strength for the eigenstates $\alpha = 1, 2$ would be negligible because of the spin selection rule. In practice the parameters φ_1 and φ_2 would be very small compared with φ_3. The value of φ_3 itself was obtained by utilizing the special solution (3.5) which reduces (3.27) to

$$\left(\frac{df^{(\rho)}}{dE} \right)_{\substack{\nu_{1/2} = -\mu_3 \\ \tau_\rho = \mu_3}} = \frac{|\varphi_3|^2}{1 - Q_{33}} \,, \quad (6.4)$$

where we have assumed tentatively that the other ρ values do not contribute appreciably at the spectral point $\nu_{1/2} = -\mu_3$; that is, (6.4) was set equal to the entire observed oscillator strength at this point. The resulting values of $df_d^{(\rho)}/dE$, plotted in Fig. 4 (dashed curve), reproduce the major features of the experimental spectrum, with the exception of the sharp peak which is known to arise mainly from s state excitations. This preliminary fitting was then improved by inserting small nonzero values of φ_1 and φ_2.

The contribution of the oscillator strength of the "s" channels cannot be attributed to a single eigenstate $\alpha = 4$ or 5, because we know from Sec. V that neither of these eigenstates has approximately triplet character. Also the absorption peak attributable to s excitation lies between the values of $\nu_{1/2} = -\mu_4$ and $-\mu_5$ (both mod 1), indicating that excitations of both eigenstates interfere constructively near the peak. On this qualitative basis the values of φ_4 and φ_5 were determined.

We proceed to a finer determination of the above five tentatively determined φ_α's from Eq. (3.27), using the parameters μ_α, $U_{\bar{4}\alpha}$, and $U_{\bar{5}\alpha}$ obtained in the earlier fitting, as listed in Table I. We note that for each value of $\nu_{1/2}$ there are three values of τ_ρ corresponding to different collision eigenstates ρ. The pairs of values ($\nu_{1/2}$, τ_ρ) have to be chosen to satisfy the consistency Eq. (3.4), $F(\nu_{1/2}, -\tau_\rho) = 0$. By trial and error a final set of φ_α's is chosen, as listed in Table I, which fit the experimental data to the extent shown in Fig. 4.

B. Discrete Spectrum

It is interesting to compare the theoretical oscillator strength formula (3.18) for a discrete line with that for photo-ionization to an eigenstate Ψ_ρ of the auto-ionization spectrum. The discrete strengths f_n are obtained from the continuum strength $df^{(\rho)}/dE$ by (i) setting $\nu_{1/2} = \nu_{1/2,n}$, (ii) replacing τ_ρ by $-\nu_{3/2,n}$, and (iii) dividing by the discrete normalization coefficient

TABLE I. Fitted values of theoretical parameters. See Sec. V for the meaning of $\bar{4}$ and $\bar{5}$ in the labeling of U-matrix elements.

α	1	2	3	4	5
μ_α	0.57	0.36	0.125	0.047	−0.007
$U_{\bar{4}\alpha}^2$	0.13	0.48	0.37	0.01	0.01
$U_{\bar{5}\alpha}^2$	0.01	0.01	0.01	0.80	0.17
$U_{\bar{4}\alpha}$	0.36	0.69	0.61	0.1	−0.1
$U_{\bar{5}\alpha}$	−0.1	−0.1	0.1	0.89	0.41
φ_α(a.u.)	0.8	−0.13	4.17	0.64	−1.19

$$\nu_{3/2,n}^3 + \nu_{1/2,n}^3 (G_{1/2,n}/G_{3/2,n}) \ . \qquad (6.5)$$

The coefficients G are defined by (3.17a) and (3.17b) and their ratio represents the slope of the $F=0$ curve according to (4.3). The normalization factor (6.5) coincides with (57) of FH. [The continuum wave function of FH is normalized per unit energy range in the auto-ionization region and thus differs from the Ψ_ρ of this paper by the square root of the expression (3.26), $G_{3/2}B_4^2$.]

Having already evaluated the theoretical expression of $df^{(\rho)}/dE$ with the values φ_α in Table I we now perform the comparison with the discrete strengths in the following way: We plot in Fig. 5 $df^{(\rho)}/dE$ vs $\nu_{1/2}$ over three periods of $\nu_{1/2}$; each period corresponds to one of the three roots τ_ρ of the Eq. (3.4) $F(\nu_{1/2}, -\tau_\rho)=0$. The corresponding root τ_ρ is plotted below the main graph of Fig. 5 for purposes of identification. (The value of df/dE plotted in Fig. 4 is the sum of the values of $df^{(\rho)}/dE$ at the three abscissas of Fig. 5 with the same value of $\nu_{1/2}$.) Each of the experimental values of f_n from Ref. 8, listed in Table II, has been divided by the appropriate value of the coefficient (6.5) and plotted in Fig. 5 (as marked by crosses) at the abscissa for which $\nu_{1/2}=\nu_{1/2,n}$ and $\tau_\rho=-\nu_{3/2,n}$.

The reduced experimental points appear to agree with the main features predicted by the theoretical curve, which was based on fitting to the auto-ionization spectrum. Note in particular:

(a) The intensities of the discrete and continuum

TABLE II. Xe level positions, line intensities, and Landé g factors.

Desig.[a,b]	Level (cm^{-1})	$\nu_{1/2}$ (mod 1)	$\nu_{3/2}$ (mod 1)	f_{expt}[c]	$\frac{df^{(\rho)}}{dE}$[d]	g_{expt}[e]
$6s[1\frac{1}{2}]^\circ$	68 045.663	0.65	0.92	0.272	1.92	1.204
$6s'[0\frac{1}{2}]^\circ$	77 185.560	0.88	0.31	0.189	2.28	1.321
$5d[0\frac{1}{2}]^\circ$	79 987.16	0.97	0.48	0.012	0.18	1.395
$5d[1\frac{1}{2}]^\circ$	83 890.47	0.12	0.81	0.381	9.0	
$7s[1\frac{1}{2}]^\circ$	85 440.53	0.19	0.98	0.09	2.37	
$6d[0\frac{1}{2}]^\circ$	88 550.28	0.35	0.44	0.002	0.1	
$6d[1\frac{1}{2}]^\circ$	90 032.65	0.45	0.75	0.082	4.76	
$8s[1\frac{1}{2}]^\circ$	90 932.939	0.51	0.99	0.021	1.33	1.182
$7d[0\frac{1}{2}]^\circ$	92 128.795	0.60	0.39	0.021	2.0	1.273
$7d[1\frac{1}{2}]^\circ$	92 714.555	0.65	0.63	0.0003	0.03	0.819
$9s[1\frac{1}{2}]^\circ$	93 422.615	0.71	0.99	0.001	0.14	1.154
$5d'[1\frac{1}{2}]^\circ$	93 618.75	0.73	0.10	0.186	38.6	
$8d[0\frac{1}{2}]^\circ$	94 228.523	0.79	0.52	0.006	1.01	1.180
$8d[1\frac{1}{2}]^\circ$	94 685.94	0.83	0.90	0.109	24.23	0.914
$10s[1\frac{1}{2}]^\circ$	94 787.603	0.84	0.001	0.015	3.31	1.164
$9d[0\frac{1}{2}]^\circ$	95 228.913	0.89	0.49			1.217
$9d[1\frac{1}{2}]^\circ$	95 498.99	0.92	0.86			0.899
$11s[1\frac{1}{2}]^\circ$	95 591.48	0.93	0.995			1.188
$7s'[0\frac{1}{2}]^\circ$	95 801.092	0.96	0.35			
$10d[0\frac{1}{2}]^\circ$	95 913.388	0.97	0.56			
$10d[1\frac{1}{2}]^\circ$	96 046.28	0.98	0.83			
$12s[1\frac{1}{2}]^\circ$	96 123.28	0.99	0.008			
$11d[0\frac{1}{2}]^\circ$	96 315.67	0.02	0.50			
$11d[1\frac{1}{2}]^\circ$	96 424.28	0.03	0.82			
$13s[1\frac{1}{2}]^\circ$	96 481.13	0.04	0.005			
$12d[0\frac{1}{2}]^\circ$	96 616.73	0.06	0.49			
$12d[1\frac{1}{2}]^\circ$	96 694.90	0.07	0.81			
$14s[1\frac{1}{2}]^\circ$	96 737.9	0.07	0.004			

[a] Reference 7.

[b] The labeling of levels in figures will be abbreviated by: $ns \equiv ns[1\frac{1}{2}]^\circ$, $ns' \equiv ns'[0\frac{1}{2}]^\circ$, $nd \equiv nd[0\frac{1}{2}]^\circ$, $n\bar{d} \equiv nd[1\frac{1}{2}]^\circ$, and $ns' \equiv ns'[0\frac{1}{2}]^\circ$.

[c] Reference 8.

[d] $df^{(\rho)}/dE = f_{expt}\{\nu_{3/2,n}^3 + [d(-\nu_{3/2})/d\nu_{1/2}]_n \nu_{1/2,n}^3\}$(a.u.).

[e] References 7 and 10.

spectra are provided by totally unrelated measurements.

(b) Reduction of the two sets of data to a comparable basis is provided here for the first time through the coefficient (6.5) and the summation of the ordinates of the three cycles of the plot of Fig. 5.

(c) The theoretical plot of $df^{(\rho)}/dE$ reproduces the main features of the experimental variations of f_n, previously unexplained. In particular it reproduces the points of near zero intensity which correspond to those intersections of the τ_ρ plots with the diagonal that indicate the occurrence of triplet eigenstates. For example note the low intensity of the $6d$ and $7\bar{d}$ lines near the collision eigenstates $\alpha = 1$ and 2, which have triplet character. The prediction of these low minima is a main feature of this theory combined with the surmise of approximate LS coupling in the eigenstates Ψ_α; we return to this point with complementary evidence in Sec. VIII.

(d) The entire fitting procedure carried out in this paper has a level of accuracy not inconsistent with the discrepancies of theory and experiment in Fig. 5.

C. Open Continuum

For $E > I_{1/2}$ the branching ratio of the two groups of photoelectrons, with kinetic energies $\frac{1}{2}k_{3/2}^2$ and $\frac{1}{2}k_{1/2}^2$, is given by (3.31). This ratio is readily calculated with the values of φ_α, μ_α, and $Q_{\alpha\beta}$ given by Table I and (5.9). We find

$$\frac{df^{(3/2)}}{dE}\Big/\frac{df^{(1/2)}}{dE} = 1.6 \tag{6.6}$$

in full agreement with the value 1.6 measured by Samson and Cairns.[6] Since the parameter φ_3 is much larger than the other φ_α, the value of (6.6) depends primarily on the ratio $P_{33}/Q_{33} = (1 - Q_{33})/Q_{33}$; in fact, it does not differ from this ratio significantly. According to (4.2) this ratio is the reciprocal of the slope of the $F = 0$ curve at the point $\nu_{1/2} = \nu_{3/2} = -\mu_3$; we have here another example of the close relationship between quantities determined in different spectral regions.

The result (6.6) and the corresponding experimental value depart significantly from the value 2 of the branching ratio which would be predicted on "statistical grounds." The statistical argument could be formulated in the context of this paper in various ways among which we mention the following one. Assuming that (a) the s and d channels are uncoupled and (b) that the α states are LS coupled, then only φ_3 and φ_5 would be nonzero, Q_{33} and Q_{55} would both equal $\frac{1}{3}$, and Q_{35} would vanish. The branching ratio would then equal $P_{33}/Q_{33} = P_{55}/Q_{55} = 2$ irrespective of the values of φ_3 and φ_5. From this point of view, the sizable departure of the branching ratio (6.6) from 2 is traceable to the seemingly small departure of $Q_{33} = 0.38$ from the value $\frac{1}{3}$ which pertains to a ^1P state.

VII. LANDÉ g FACTOR

Values of the Landé factor, measured by Zeeman-effect experiments for many of the discrete levels considered in this paper,[7,10] are listed in Table II. The measured value of this factor for each discrete level, g_n, represents the expectation value of the operator $g = 1 + \vec{S}\cdot\vec{J}/\vec{J}\cdot\vec{J}$ over the level's wave function Ψ_n,

$$g_n = \int \Psi_n^\dagger g \Psi_n d\tau \Big/ \int |\Psi_n|^2 d\tau \ . \tag{7.1}$$

In this paper the wave functions Ψ_n have been determined only to an extent insufficient for the evaluation of (7.1). First, the expression (2.17) holds only for $r > r_0$; this limitation is not too serious because the region $r > r_0$ yields presumably most of the contribution to the integrals in (7.1) for excited states of the atom. Second, we have obtained only two rows of matrix elements, $U_{\bar{4}\alpha}$ and $U_{\bar{5}\alpha}$, which include seven independent parameters out of the total of ten required to determine the complete matrix $U_{i\alpha}$. [In addition the matrix rows labeled $\bar{4}$ and $\bar{5}$ in Sec. V coincide only approximately with $i = 4$ and 5 as defined by (2.11).] Nevertheless, a few steps of the evaluation of (7.1) will be outlined here to demonstrate how to utilize additional information as it becomes available.

The denominator of (7.1) can be taken from (3.13). In the numerator, the operator g acts only on the angular and spin factors Φ_i of the wave function (2.17) and is accordingly represented by the matrix

$$i = \begin{pmatrix} 1 & 2 & 3 & 4 & 5 \end{pmatrix}$$

$$g_{ij} = \begin{pmatrix} \frac{11}{10} & \frac{-3}{10} & 0 & 0 & 0 \\ \frac{-3}{10} & \frac{16}{15} & 0 & \frac{1}{6}\sqrt{5} & 0 \\ 0 & 0 & \frac{7}{6} & 0 & \frac{1}{6}\sqrt{2} \\ 0 & \frac{1}{6}\sqrt{5} & 0 & \frac{5}{6} & 0 \\ 0 & 0 & \frac{1}{6}\sqrt{2} & 0 & \frac{4}{3} \end{pmatrix}. \tag{7.2}$$

For the purposes of radial integration we note that the form (2.17) of the wave function simplifies considerably for levels of the discrete spectrum, with parameters $\nu_{1/2,n}$, $\nu_{3/2,n}$, and $A_\alpha^{(n)}$ which satisfy the Eqs. (2.18). In this case one finds

$$\Psi_n = \sum_i \Phi_i y_5(\nu_{in}, r) \frac{\Gamma(l_i + 1 - \nu_{in})}{\pi \nu_{in}^{l_i}} \sum_\alpha U_{i\alpha} \sin\pi\mu_\alpha A_\alpha^{(n)} \ , \tag{7.3}$$

where

$$y_5(\nu, r) = W_{\nu, l+1/2}(2r/\nu) \tag{7.3'}$$

is the exponentially decreasing Whittaker function used in Ref. 2. Substitution of (7.3) yields

$$\int \Psi_n^\dagger g \Psi_n d\tau \approx \sum_{ij} g_{ij} \int_{r_0}^{\infty} y_5(\nu_{in}, r) y_5(\nu_{jn}, r) dr$$

$$\times \frac{\Gamma(l_i+1-\nu_{in})}{\pi\nu_{in}^{l_i}} \sum_\alpha U_{i\alpha} \sin\pi\mu_\alpha A_\alpha^{(n)}$$

$$\times \frac{\Gamma(l_j+1-\nu_{jn})}{\pi\nu_{jn}^{l_i}} \sum_\beta U_{j\beta} \sin\pi\mu_\beta A_\beta^{(n)} \ . \quad (7.4)$$

VIII. DISCUSSION

Several relationships have been established in this paper between spectral properties of Xe in the discrete and continuum regions. The plot of the consistency equation $F(\nu_{1/2}, \nu_{3/2}) = 0$, in Fig. 2, determines on the one hand the position of discrete levels of strongly perturbed series and on the other hand the resonant behavior of collision eigenphases $\pi\tau_\rho$ in the auto-ionization region. Figure 5 of τ_ρ in the lower plot, is associated with maxima of oscillator strengths. The main upper portion of Fig. 5 provides the connection between the oscillator strengths in the discrete and the continuum, on the same scale. Finally, the data obtained from the lower portion of the spectrum have provided an interpretation of the branching ratio (6.6) measured in the open continuum (above the second threshold $I_{1/2}$). In all these regards the series of discrete levels and their adjoining continua can be indeed treated as a single unit.

The analytical treatment of this paper involves the parameters μ_α, D_α, and $U_{i\alpha}$. Values of the ten parameters μ_α and D_α (or, rather, of the equivalent φ_α) have been obtained by fitting 28 discrete level positions and the profile of auto-ionization lines and are given in Table I. This table also gives values of matrix elements $U_{\bar{4}\alpha}$ and $U_{\bar{5}\alpha}$ obtained by the same fitting procedure, which amount to seven out of the ten independent data required to determine the matrix $U_{i\alpha}$. However, the problem of indeterminacy of $U_{i\alpha}$ exists as mentioned in Sec. III. Additional effort will be required to obtain the remaining parameters and thus to calculate the Landé factors g_n as well as the angular distribution of photoelectrons. Extension of the treatment presented here to channels with different J values, as outlined in the Appendix, and with different l quantum numbers of the dissociating electron would permit a calculation of the cross sections for elastic and inelastic $e + Xe^+$ collisions at low energies.

Observable properties have been related here to the five close-coupling eigenchannels of the complex $e + Xe^+$. A preliminary characterization of these eigenchannels has been achieved. In three of them the electron's orbital momentum is 98% $l = 2$, and 2% $l = 0$; in the other two the situation is reversed. Yet the s-d interference effects are quite appreciable, being of order $\approx (0.01)^{1/2}$ as characterized by the small elements $U_{\bar{4}\alpha}$ or $U_{\bar{5}\alpha}$, i.e., roughly 10%, and are clearly observed in the avoided crossings of Fig. 2. One of the three eigenchannels with predominantly d character, namely, the one labeled by $\alpha = 3$, is identified as predominantly singlet by the large value of the intensity parameter φ_3^2 and the local maximum of oscillator strength at $\nu_{1/2} = -\mu_3 = 0.875$ (mod 1) in Fig. 5. The triplet character of the channels $\alpha = 1$ and $\alpha = 2$ is supported by the minima of strength at $\nu_{1/2} = -\mu_1 = 0.43$ and $\nu_{1/2} = -\mu_2 = 0.64$ (mod 1) in Fig. 5.

This interpretation of apparent anomalies of oscillator strengths along perturbed spectra, illustrated by Fig. 5, constitutes a main result of this paper. As a further illustration to show the potential of this analysis we list in Table III relative intensities of absorption lines in Ar measured recently by Yoshino.[20] Partial data for argon are shown for three of the same five series as occur in Xe, together with the value of $\nu_{1/2} - \nu_{3/2}$ for each line. The intensities of these three series are seen to drop as the value of $\nu_{1/2} - \nu_{3/2}$ passes through zero (mod 1); the values of $-\nu_{1/2}$ (mod 1) at which this drop occurs represent values of μ_α for eigen-

TABLE III. Ar relative line intensities.

$ns[1\frac{1}{2}]_1^{\circ}$ [a]	I [a]	$\frac{\nu_{1/2}-\nu_{3/2}}{\tau_{\rho n}+\nu_{1/2,n}}$ (mod 1)	$nd[1\frac{1}{2}]_1^{\circ}$ [a]	I [a]	$\frac{\nu_{1/2}-\nu_{3/2}}{\tau_{\rho n}+\nu_{1/2,n}}$ (mod 1)	$nd[0\frac{1}{2}]_1^{\circ}$ [a]	I [a]	$\frac{\nu_{1/2}-\nu_{3/2}}{\tau_{\rho n}+\nu_{1/2,n}}$ (mod 1)
5	70	0.86	12	42	0.16	11	35	0.72
6	56	0.67	13	60	0.37	12	30	0.61
7	41	0.39	14	45	0.54	13	29	0.37
8	42	0.001 [b]	15	34	0.69	14	22	0.18
9	41	0.54	16	29	0.83	15	9	0.0
10	15	0.99 [b]	17	18	0.98 [c]	16	23	0.12
11	30	0.36	18	41	0.89	17	34	0.13
12	42	0.68	19	40	0.03 [c]	18	30	0.03
13	28	0.95	20	59	0.11	19	30	0.31
14	30	0.17	21	41	0.18	20	29	0.41
15	60	0.36	22	36	0.24	21	28	0.49

[a] Classification and intensity from Ref. 20.

[b] These two lines have values of $\nu_{3/2}$ differing by ≈ 0.03 and correspond to different eigenchannels, presumably s^1P and s^3P.

[c] These two lines correspond to different eigenchannels, presumably d^3P and d^1P.

channels with triplet character according to LS coupling. A singlet character eigenchannel does not cause a drop in intensity as the value of $\nu_{1/2} - \nu_{3/2}$ passes through zero (see, for example, $8s[1\frac{1}{2}]^\circ$ level in Table III).

The further characterization of the eigenchannels $\alpha = 1$ and $\alpha = 2$ as ^3P and ^3D, respectively, requires additional evidence. This evidence is provided in the Appendix by the plots of levels $5p^5nd$ and $5p^5ns$ but with $J \neq 1$. These plots support the statement that the character of LS-coupled eigenchannels α is essentially the same for different J values. For example, the fact that the $J = 3$ plots in Fig. 6(c) do not intersect the diagonal near $\nu_{1/2} = 0.43$ shows that $\alpha = 1$ is part of an LS multiplet without any $J = 3$ level. The data in the Appendix also confirm the other assignments made in this paper.

As noted in Sec. V the LS characterization breaks down for the two eigenchannels with s character, namely, $\alpha = 4$ and 5. This breakdown is understood qualitatively on the basis of the relative strength of spin-orbit coupling and electrostatic interaction. In our collision method, interaction strengths are represented by dimensionless numerical parameters equal to the shifts of quantum defect $\Delta\mu$ they produce. On this scale the strength of the spin-orbit coupling in the Xe^+ ion doublet is represented by $\Delta\mu_{so} = 0.049$.[21] On the other hand the quantum-defect differences $\mu_\alpha - \mu_\beta$ of the close-coupling eigenchannels should arise primarily from electrostatic interaction and should be at least of the order of 0.1 for Xe. These differences are $\gtrsim 0.2$ for the eigenchannels with d character, i.e., with $(\alpha, \beta) = 1, 2, 3$, and thus are much larger than $\Delta\mu_{so} = 0.049$. However for the eigenchannels $\alpha = 4, 5$ with s character this difference is $\mu_4 - \mu_5 = 0.05$, which is comparable with the strength of the spin-orbit coupling. The large effect of spin-orbit coupling on the eigenchannels $\alpha = 4, 5$ is then attributed to an anomalously small value of the sp exchange electrostatic interaction[22] which would otherwise widen the difference analogous to $\mu_4 - \mu_5$. In fact, the quantum-defect difference analogous to $\mu_4 - \mu_5$ ranges between 0.03 and 0.05 for all other noble gases; in the other gases this value is larger than spin-orbit effect $\Delta\mu_{so}$, which is smaller than for Xe. Thus the LS characterization for the eigenchannels with s character is better fulfilled for other noble gases than for Xe.

As emphasized in Sec. I and in LF, the energy dependence of the parameters μ_α, $U_{i\alpha}$, and φ_α has been disregarded altogether in the fitting of data. Gross misfitting due to this rather extreme schematization is apparent *only* in the position of the $6s$ and $6s'$ levels, which lie about 0.06 units outside the $F = 0$ curve of Fig. 2; a lesser misfit by 0.01 is observed for the $7s$ level. These misfits may be interpreted in terms of an upward drift of μ_4 and μ_5 as the energy E decreases.[12] The absence of a corresponding upward drift of the μ_α values for the d channels in Xe may be due to a centrifugal barrier effect.

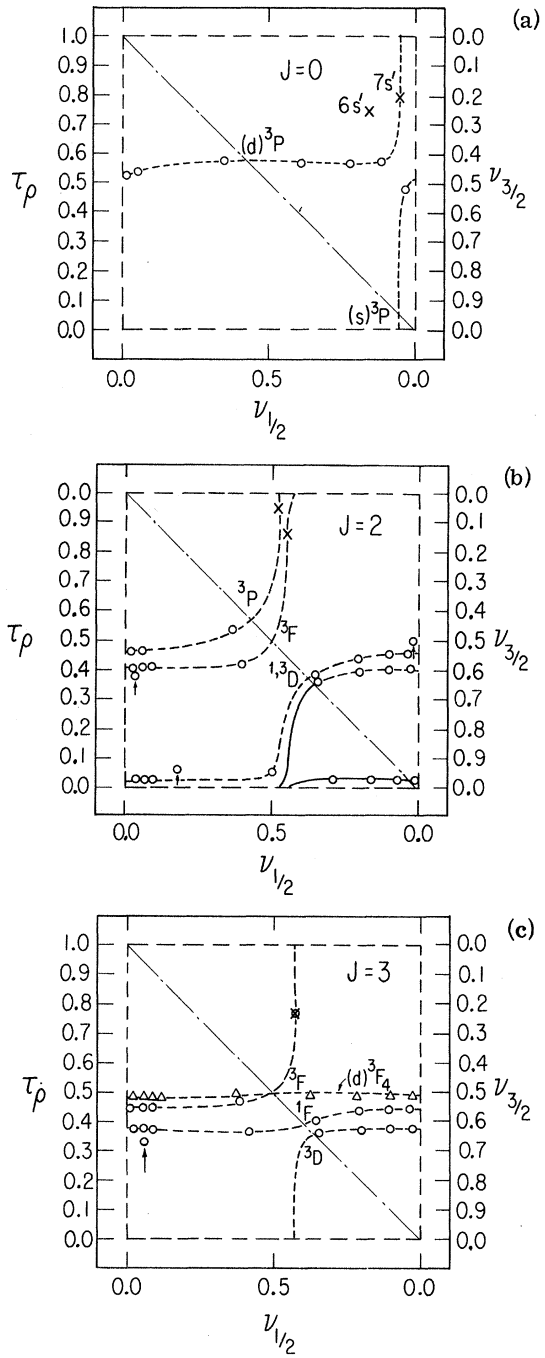

FIG. 6. Plot of $\nu_{3/2}$ or τ_ρ vs $\nu_{1/2}$ as in Fig. 2 with different J values. (a): $J = 0$ with LS-coupled states s^3P_0 and d^3P_0. (b): $J = 2$ with LS-coupled states s^3P_2, d^3P_2, d^1D_2, d^3D_2, and d^3F_2. (c): 0, $J = 3$ with LS-coupled states d^3D_3, d^1F_3, and d^3F_3; Δ, $J = 4$ with LS-coupled state d^3F_4. Dashed lines are interpolated curves.

Accounting quantitatively for the values of the μ_α, D_α and for the coupling characteristics of the eigenchannels Ψ_α should be the objectives of calculations by the close-coupling[23] or equivalent methods. The semiempirical approach developed in this paper may be extended to higher accuracy, e.g., by improved fitting and by taking care of the energy dependence of the parameters. Complementary information could be obtained from experimental analysis of the angular distribution of photoelectrons, particularly in the auto-ionization region where the distribution must vary periodically along the spectrum. The plots in Fig. 5 may serve as a guide for future line intensity measurements for highly excited and strongly perturbed levels. Extended information should be gathered readily by applying the analysis of this paper to the spectra of the other noble gases. On the other hand a substantial amount of further development will be required for application to the photoabsorption spectra of atoms that have more than two ionization thresholds within 3–4 eV of the lowest one.

Finally, we compare the approach of this paper with the traditional interpretation of auto-ionization spectra and of series perturbation in terms of configuration interaction.[18] Configuration interaction normally deals with the perturbation of a continuous spectrum or of a Rydberg series by a *single discrete* level of a different series. Initial steps have been taken in the past to deal simultaneously with the perturbations caused by a series of Rydberg levels, but the formalism did not appear suitable unless the perturbing levels were well separated. The formalism of configuration interaction maintains a clear distinction between a perturbing level, or series of levels, and the perturbed series. In the present approach all interactions are regarded as included in the characterization (a) of the close-coupling eigenchannels Ψ_α and of their quantum defects μ_α, and (b) of dissociation channels Ψ_i and of their ionization thresholds $I_{3/2}$ and $I_{1/2}$. The present theory deals with the frame transformations $U_{i\alpha}$ between the states Ψ_α and Ψ_i as well as with the effects of the Coulomb field on the excited electron, which yield the entire Rydberg structure. Configuration interaction and its effect of auto-ionization do not appear explicitly here but their consequences emerge from the expression of the expansion coefficients A_α and from the values of the quantum defects μ_α.

ACKNOWLEDGMENT

This work owes much to the continued help and guidance from Professor U. Fano. I wish to acknowledge the important contributions due to Professor Fano to this work particularly in Secs. II, III, and VIII and to express my gratitude to him.

APPENDIX

In the text we have considered only $J=1$ states which are reached from the ground state, $5p^6\,{}^1S_0$, by way of electric dipole transitions. However, the angular momentum coupling of an s or d electron to the $5p^5\,{}^2P_{1/2,3/2}$ core can also produce states with $J=0$, 2, 3, and 4 and with the same thresholds $I_{3/2}$ or $I_{1/2}$[7] as for $J=1$. The close-coupling eigenchannels with these alternative values of J should be related to those with $J=1$. To be specific, *the character of the LS-coupled eigenchannels should be the same irrespective of the J values.*

The plots $\nu_{3/2,n}$ vs $\nu_{1/2,n}$ for observed levels with different J values are shown in Fig. 6. The LS-coupled states belonging to a given J are listed on each figure. The intersections of the interpolated curve with the diagonal line give the eigenphases $\pi\mu_\alpha$. Figure 6(a) shows the case of $J=0$ for which there are just two dissociation channels, namely, $p^5(^2P_{1/2})s$ with the threshold $I_{1/2}$ and $p^5(^2P_{3/2})d$ with threshold $I_{3/2}$. In LS coupling these channels can form only ^3P states. The interpolated curve passes through the diagonal line at $\nu_{1/2}\approx 0.43$ (mod 1). This corresponds to a collision eigenstate p^5d^3P in LS coupling with eigenphase $\mu_\alpha = 0.57$. In both Fig. 6(b) for $J=2$ states and Fig. 2 for $J=1$ states, we note that intersections occur at the same place $\nu_{1/2} \approx 0.43$, which corresponds to a p^5d^3P eigenstate. Here, at least, the eigenphase is the same for the same eigenchannel α independently of the J value. The other intersection with the diagonal occurs in Fig. 6(a) at $\nu_{1/2}\approx 0.95$, i.e., near the value of $-\mu_4$ for $J=1$. A series of states of the $p^5(^2P_{1/2})s$ channel intersects the diagonal in Fig. 6(b) for $J=2$ at $\nu_{1/2} \approx 0.98$, that is, at a point intermediate between those of $\alpha=4$ and $\alpha=5$ for $J=1$. The intersection corresponding to ^3D occurs at $\nu_{1/2}\approx 0.64$ for $J=3$, while for $J=2$ intersections corresponding to ^3D or ^1D occur between $\nu_{1/2}\approx 0.62$ and 0.65, that is, near the $\nu_{1/2}\approx 0.64$ attributed to $^3D_1$ in Fig. 2 for the $J=1$ plot.

The assignments of the eigenchannels at the other intersections are also consistent with the LS scheme, e.g., $\nu_{1/2}\approx 0.5$ is attributed to ^3F in Fig. 6(b) for $J=2$ and in Fig. 6(c) for $J=3$ and $J=4$.

---

*Work supported by the U. S. Atomic Energy Commission, Contract No. C00-1674-40.

†Presented as a thesis to the Department of Physics, The University of Chicago, in partial fulfillment of the requirements for the Ph. D. degree.

‡Present address: Department of Physics, University of Arizona, Tucson, Ariz. 85721.

[1]See, for example, L. Fonda and R. G. Newton, Ann. Phys. (N. Y.) 9, 416 (1960); M. H. Ross and G. L. Shaw, *ibid.* 13, 147 (1961); and M. Gailitis, Zh.

Eksperim. i Teor. Fiz. 44, 1974 (1963) [Sov. Phys. JETP 17, 1328 (1963)].

[2]M. J. Seaton, Proc. Phys. Soc. (London) 88, 801 (1966).

[3]U. Fano, Phys. Rev. A 2, 353 (1970).

[4]K. T. Lu, Bull. Am. Phys. Soc. 13, 37 (1968).

[5]K. T. Lu and U. Fano, Phys. Rev. A 2, 81 (1970).

[6]J. A. R. Samson and R. B. Cairns, Phys. Rev. 173, 80 (1968).

[7]C. E. Moore, *Atomic Energy Levels*, Natl. Bur. Std. (U. S.) Circular No. 467 (U. S. GPO, Washington, D. C., 1958), Vol. III.

[8]S. Natali, C. E. Kuyatt, and S. R. Mielczarek (unpublished). The line intensities are measured by electron spectroscopy. (We express our appreciation to Dr. Kuyatt for allowing us use of the data before publication.)

[9]R. E. Huffman, Y. Tanaka, and J. C. Larrabee, J. Chem. Phys. 39, 910 (1963); and R. E. Huffman, Air Force Cambridge Research Laboratory Report No. 64-911 (unpublished); and Physical Sciences Research Papers No. 66 (unpublished).

[10]P. G. Wilkinson, Can. J. Phys. 45, 1709 (1967).

[11]An interaction matrix element between discrete states with effective quantum number n^* and n'^* is usually renormalized by multiplication by $(n^*n'^*)^{3/2}/27.2$ eV. This procedure amounts to calculating the ratio of the interaction to the interval of successive Rydberg levels. See, for example, H. A. Bethe, *Intermediate Quantum Mechanics* (Benjamin, New York, 1964), pp. 29–30.

[12]Effects of the variation of μ are discussed in Ref. 2; FH, Appendix B; and A. F. Starace (unpublished).

[13]Stationary state wave functions of the scattering process $e + Xe^+$ are often written in the general form

$$\sum_{ij} \Phi_i [f(\nu_i, r)\delta_{ij} - g(\nu_i, r)R_{ij}]h_j ,$$

where $R_{ij} = \sum_\alpha U_{i\alpha} \tan\pi\mu_\alpha U^\dagger_{\alpha j}$ is a reaction matrix and the h_j are arbitrary coefficients. This equation reduces to (2.16) by setting $h_j = U_{j\alpha} \cos\pi\mu_\alpha$, meaning that $c_i = h_i$ and $d_i = \sum_j R_{ij}h_j$.

[14]U. Fano, Bull. Am. Phys. Soc. 13, 37 (1968).

[15]Note that the scale of the graph in units of the effective quantum numbers $\nu_{1/2}$ indicates interaction strengths on an absolute scale, on which unity represents the limit of strong interaction.

[16]J. H. Macek, Phys. Rev. A 2, 1101 (1970).

[17]H. Feshbach, Ann. Phys. (N. Y.) 43, 410 (1967); F. H. Mies, Phys. Rev. 175, 164 (1968).

[18]U. Fano, Phys. Rev. 124, 1866 (1961).

[19]F. J. Comes and H. G. Sälzer, Phys. Rev. 152, 29 (1966).

[20]K. Yoshino, J. Opt. Soc. Am. 60, 1220 (1970).

[21]U. Fano, Comments At. Mol. Phys. II, 30 (1970).

[22]E. U. Condon and G. H. Shortley, *The Theory of Atomic Spectra* (Cambridge U. P., New York, 1964), pp. 301–305.

[23]P. Burke, *The Physics of Electrons and Atomic Collisions, Invited Papers from the Fifth International Conference*, edited by L. M. Branscomb (Joint Institute for Laboratory Astrophysics, University of Colorado, Boulder, Colo., 1968).

PHYSICAL REVIEW A VOLUME 4, NUMBER 2 AUGUST 1971

Vibrorotational Excitations of H_2^+ by e^+ Impact. I

F. H. M. Faisal*
Laboratory for Space Physics, Goddard Space Flight Center, Greenbelt, Maryland 20771
(Received 17 December 1970)

Analogies between Coulomb excitations of nuclei and ionic molecules by charged projectiles are utilized to calculate vibrorotational excitations of H_2^+ molecular ions by e^+ impact by a semiclassical method developed in the nuclear case. The coupling between vibrational-rotational states of target molecules can very significantly affect the scattering cross sections for either kind of excitation on the other. In this paper we have shown that the effect of such coupling may be included very conveniently, under the present model, whenever applicable. In a subsequent paper we intend to publish results for the experimentally more accessible systems, including the $H^+ + H_2^+$ system.

I. INTRODUCTION

Recently there has been a considerable upsurge of interest in the study of rotational and vibrational energy-loss processes in diatomic molecules by electron impact. They are of much importance not only for understanding the fundamental energy exchange processes involved, but also for their applications in such allied fields as astrophysics and atmospheric physics.

In the present work we shall investigate the coupled excitation of vibrorotational states of hydrogen molecular ions H_2^+ by collision with positrons e^+. The study of such excitations with e^+ is not only important for its intrinsic significance but also for the mathematical simplicity it introduces in the formulation of the complex excitation process itself. This is due to the fact that the Pauli exchange does not enter directly into the problem.

In this work we shall adopt a semiclassical view and make use of the analogy of Coulomb excitations of nuclei, which has been studied extensively in the past.[1] The present method is semiclassical in that we shall treat the target system quantum mechanically while the motion of the projectile would be